12-2012

Silica Nanoparticle-Based Coatings with Superhydrophilic and Superhydrophobic Properties

Robert Andrew Fleming
University of Arkansas, Fayetteville

SILICA NANOPARTICLE-BASED COATINGS WITH SUPERHYDROPHILIC AND SUPERHYDROPHOBIC PROPERTIES

SILICA NANOPARTICLE-BASED COATINGS WITH SUPERHYDROPHILIC AND SUPERHYDROPHOBIC PROPERTIES

A thesis submitted in partial fulfillment
of the requirements for the degree of
Master of Science in Mechanical Engineering

By

Robert A. Fleming
University of Arkansas
Bachelor of Science in Mechanical Engineering, 2009

December 2012
University of Arkansas

ABSTRACT

Superhydrophilic and superhydrophobic surfaces have potential for implementation into a variety of fields, including self-cleaning surfaces, anti-fogging transparent materials, and biomedical applications. In this study, sandblasting, oxygen plasma treatments, silica nanoparticle films, and a low surface energy fluorocarbon film were employed to change the natural surface wettability of titanium, glass, and polyethylene terephthalate (PET) substrates, with an aim to produce superhydrophilic and superhydrophobic behavior. The effects of these surface modifications are characterized by water contact angles (WCAs), surface wetting stability, surface morphology and roughness, surface elemental composition, and optical transmittance measurements. The results show that stable superhydrophilic and superhydrophobic surfaces can be fabricated on titanium; stable superhydrophilic and unstable nearly superhydrophobic surfaces can be fabricated on glass; and very hydrophilic (WCA ~ 10°) and very hydrophobic (WCA ~ 135°) surfaces can be produced on PET. In addition, the silica nanoparticle films utilized have antireflective properties and increase optical transmittance of glass and PET substrates across the entire visible spectrum. This thesis provides a foundation for further studies into the implementation of these functional surfaces into practical applications, as well as a deeper understanding of how the properties (morphology, roughness, chemistry, etc.) of these modified surfaces influence their surface wetting properties.

This thesis is approved for recommendation
to the Graduate Council.

Thesis Director:

_____

Dr. Min Zou

Thesis Committee:

_____

Dr. Douglas Spearot

_____

Dr. Po-Hao “Adam” Huang

THESIS DUPLICATION RELEASE

I hereby authorize the University of Arkansas Libraries to duplicate this thesis when needed for research and/or scholarship.

Agreed _____
Robert Fleming

Refused _____
Robert Fleming

ACKNOWLEDGMENTS

I would like to thank Dr. Min Zou for her support and guidance as my advisor, as well as Dr. Douglas Spearot and Dr. Adam Huang for serving on the thesis committee. In addition, I would like to thank the staff of the High Density Electronics Center (HiDEC), especially Errol Porter, for cleanroom equipment support, as well as Dr. Mourad Benamara and Dr. Mike Hawkridge of the Electron Optics Facility for analytical equipment support. This work was funded in part by the National Science Foundation (NSF) through grants CMS-0600642, CMS-0645040, EPS-1003970, and DMR-0520550, the Arkansas Biosciences Institute, and an NSF Graduate Research Fellowship under Grant No. DGE-0957325.

TABLE OF CONTENTS

I. INTRODUCTION

1.1 Background

1.1.1 Surface Wetting, Surface Free Energy, and Water Contact Angles

Surface wetting refers to the interactions between a solid and a liquid at the solid-liquid interface that is formed due to physical contact between these two phases. At the most fundamental level, the nature of these interactions are of atomic origin and represent a dynamic energy balance between intermolecular, electrostatic, polar, and gravitational energy contributions [1]. As a result of these energy contributions, a liquid droplet, upon contacting a solid surface, will adopt a geometric configuration that minimizes the total energy of the solid-liquid system [2].

The relevant energy parameter for this situation, which encompasses all of the aforementioned energetic contributions to surface wetting, is the surface free energy (SFE), defined as the reversible work required to create a unit of new surface area [3]. This parameter has units of [Energy/(Length)^2], or equivalently, [Force/Length], which are the conventional units for liquid surface tension. For a liquid, the SFE and surface tension are synonymous. In the case that the "new surface" created is interfacial surface area between the solid and liquid, the SFE is termed the solid-liquid interfacial energy.

Based on these energy considerations, the shape of a liquid droplet contacting a solid surface can be calculated from a thermodynamic energy balance. Consider a liquid droplet spreading on a solid surface, as shown in Figure 1. In this system, the vapor component is an arbitrary atmosphere, which can be either gaseous or a second immiscible liquid, and is not

necessarily the vapor-phase of the liquid component. Here, θ is defined as the water contact angle (WCA). It is limited to values between 0° and 180°, and has a geometrical interpretation as the angle between the wetted solid surface and the tangent line along the droplet at the solid-liquid-vapor interface. In practice, any liquid may be used; however, water is a frequently used liquid in contact angle measurements.

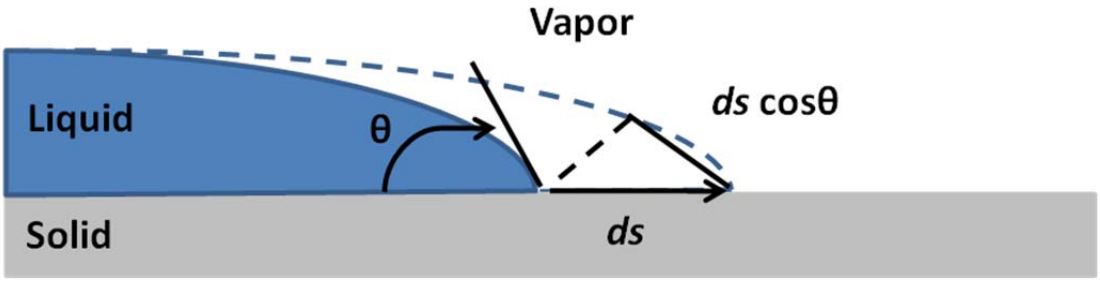

Figure 1: Schematic of a liquid droplet spreading on a solid surface, showing the WCA θ and the increase in solid-liquid interfacial area and liquid surface area.

As the liquid droplet advances outward an infinitesimal distance, it covers an area *ds* and creates new solid-liquid interfacial area of *ds* and new liquid surface area of $ds\cos\theta$. Note that the creation of new solid-liquid interfacial area results in the removal of solid surface area by the same amount. If γ_{SV}, γ_{LV}, and γ_{SL} are the SFE of the solid, the surface tension of the liquid, and the solid-liquid interfacial energy, respectively, then this results in an equilibrium energy balance

$$\gamma_{SL}ds + \gamma_{LV}ds\cos\theta - \gamma_{SV}ds = 0 \quad (1)$$

This can be rearranged to form the Young Equation, which expresses the WCA explicitly in terms of the surface energy parameters, as

$$\cos\theta = \frac{\gamma_{SV} - \gamma_{SL}}{\gamma_{LV}} \quad (2)$$

An alternative derivation of the Young Equation can be achieved by considering a force balance on the surface forces due to surface energies at the solid-liquid-vapor interface, as in Figure 2. Since all the forces share a contact line, a force balance (per unit length) produces

$$\gamma_{SV} = \gamma_{SL} + \gamma_{LV} \cos\theta \tag{3}$$

which is can be rearranged to obtain the Young Equation by a second method.

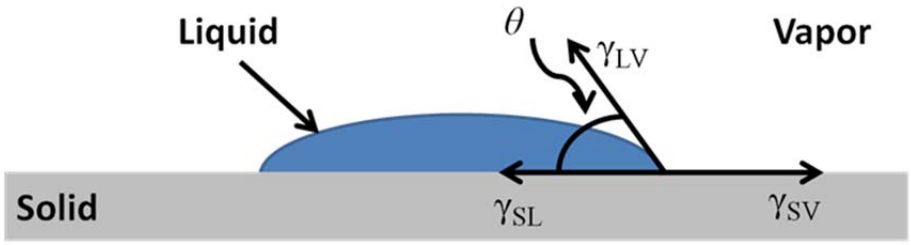

Figure 2: A model solid-liquid system, showing the surface forces acting at the solid-liquid-vapor interface.

The utility of the Young Equation is not immediately apparent. If all of the relevant surface energy parameters are known, then the geometrical shape of a liquid droplet on a solid surface can be predicted. However, in practice, all of the surface energy parameters will not be known. If only a single surface energy parameter is unknown, then an experimental measurement of the WCA can be used to calculate the unknown energy parameter. In this case, the unknown parameter is often γ_{SV}, the SFE of the solid, and measurements of SFEs of solids from contact angle measurements have precedence in the literature [4]. Even if multiple parameters are unknown, knowledge of the WCA from experimental measurements can provide qualitative information about the SFE.

1.1.2 Contact Angle Regimes

Surface wetting behavior can be broken into 4 different regimes, based on the value of WCA. The two most conventional regimes are the hydrophilic and hydrophobic regimes, defined as WCAs in the range of $10° < \theta < 90°$ and $90° < \theta < 150°$, respectively. The wetting behavior of these two regimes is fairly uninteresting, and neither regime tends to have any desirable properties compared to the other. In terms of thermodynamics, higher SFEs lead to more hydrophilic behavior, and thus smaller WCAs. The other regimes, which describe the extremes of surface wetting behavior, are wholly more interesting. Superhydrophilicity, which is characterized by WCAs in the range $\theta < 10°$, within 1 s of the initial wetting, describes nearly perfect wetting. In contrast, superhydrophobicity, described by WCAs of $\theta > 150°$, describes a state of nearly perfect non-wetting. The most striking consequence of these extreme wetting/non-wetting regimes is the opportunity to control adhesion at the solid-liquid interface. For this system, the work of adhesion can be estimated with the Young-Dupré Equation [3]

$$W_{adh} = \gamma_{LV}(1+\cos\theta) \tag{4}$$

It can be seen from Eq. (4) that, for superhydrophilic surfaces, the work of adhesion approaches twice the value of the liquid surface tension, while for superhydrophobic surfaces, the work of adhesion becomes increasingly negligible as the WCA increases.

1.1.3 Modification of Surface Free Energies

Although most raw materials have surface energies that result in simple hydrophilic/hydrophobic behavior, methods exist to modify the natural SFE of materials. These methods fall into two very broad categories: changes in surface topography and changes in surface chemistry.

The Young Equation was based on the concept of an idealized, atomically smooth solid surface. However, all surfaces have defects and imperfections that contribute to surface roughness, and this roughness will contribute to the surface wetting behavior. In view of this roughness-induced wettability modification, two well-established models have been developed to account for these effects: the Wenzel model [5] and the Cassie-Baxter model [6].

The Wenzel model accounts for the complete wetting a roughened solid surface through the equation

$$\cos\theta^* = r\cos\theta \tag{5}$$

where θ^* is the observed contact angle, θ is the WCA on a perfectly smooth surface of identical surface chemistry, and r is a surface roughness parameter defined as the ratio of the roughened surface area to the projected surface area. For any roughened surface, $r > 1$, and r increases as the surface roughness increases. The Wenzel model predicts that a hydrophilic material will become more hydrophilic as the surface roughness increases, which makes intuitive sense. However, it also predicts that a hydrophobic material will become more hydrophobic, which makes less intuitive sense, but has also been experimentally verified [7]. A major limitation of the Wenzel model is the phenomenological nature of the roughness parameter r. By definition, r can be arbitrarily large, but the presence of trigonometric terms in the Wenzel model equation places a mathematical limit on r to insure that $\cos\theta^*$ remains defined; this limit has no physical justification. For this reason, only the qualitative, and not the quantitative, behavior of the Wenzel model is significant.

The Cassie-Baxter model treats the roughened solid surface as a "composite" surface consisting of roughened material and thermodynamically-stable air-filled pores. For a generalized composite surface, the observed contact angle is

$$\cos\theta^* = f_1 \cos\theta_1 + f_2 \cos\theta_2 \tag{6}$$

where f_i is the fraction of surface area corresponding to component i. If the second component of the composite is air, as in the Cassie-Baxter model, and is assumed to have a contact angle of 180°, then the result is the Cassie-Baxter formula

$$\cos\theta^* = f(\cos\theta + 1) - 1 \tag{7}$$

where f is an areal surface fraction defined as the ratio of the wetted surface area to the total surface area, and θ^* and θ are the same as previously defined. For any surface, $f \leq 1$, and can potentially be very small, which will result in a very large WCAs. In contrast with the Wenzel model, the physical definition of f is compatible with the mathematical conditions for $\cos\theta^*$ to be defined, so no extraneous, non-physical constraints on the value of f are needed. Schematic representations of both Wenzel and Cassie-Baxter wetting behavior are shown in Figure 3.

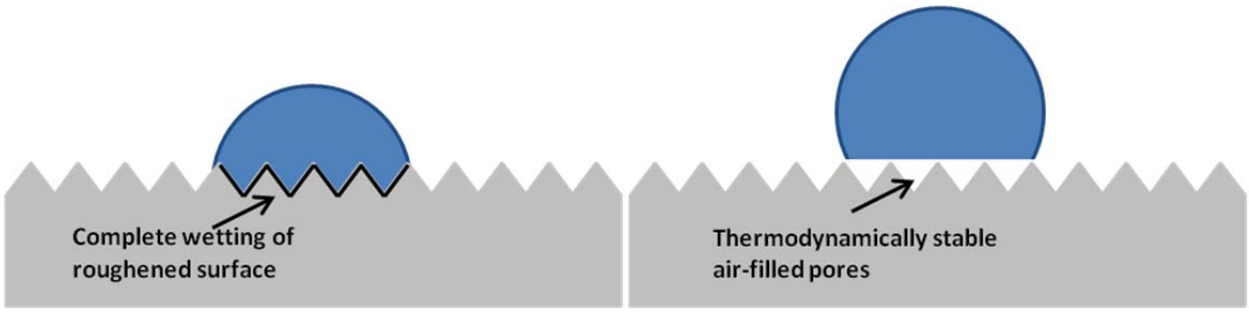

Figure 3: Schematics of Wenzel (left) and Cassie-Baxter (right) wetting behavior.

Modification of surface chemistry can be achieved in a number of ways, at a number of different length scales. Chemical functionalization, which is the attachment of molecules with desirable properties to specific surface sites through covalent bonds, changes the surface chemistry at the molecular scale. Although robust, this method requires potentially complicated chemical synthesis to produce the desired surface properties. An alternative approach is the use of self-assembled monolayers (SAMs) [8], which replaces the surface of a material with a monolayer of molecules with a different surface chemistry [9]. SAMs are deposited on a material in a liquid-phase solution, and as the solvent containing the active material evaporates, the SAM molecules will self-assembled due to van der Waals interactions and chemisorption. The best quality SAMs will be true monolayers; poorer quality SAMs may not achieve complete monolayer surface coverage or may be thicker than a monolayer, but may still have desirable surface properties. Much like chemical functionalization, preparation of the highest quality SAMs may require extensive chemical synthesis and complicated processing procedures. Yet another method of changing surface chemistry is through surface coatings [10, 11], in which the material surface is coated with a thin- or thick-film layer of a different material. These coatings have thicknesses in the range of 10s of nm to 100s of μm (or larger), far larger than the length scales of either chemical functionalization or SAMs.

1.2 Motivation

Much research activity has been directed to modifying the natural wettability of materials to a superhydrophilic or superhydrophobic state in order to take advantage of the properties of these extreme wetting states. Modified surface wetting behavior has shown much promise for the development of self-cleaning and anti-fogging surfaces [12], as well as to be integrated into

microfluidic devices [13] as alternative method to control the movement of small quantities of fluid [14]. In addition, modified surface wettability has shown to be of benefit in biomedical fields, such as prosthetic dentistry [15], improving vascular stents [16], and cell adhesion [17], as well as water-repellant insulators for electrical power systems [18], anti-icing coatings [19], water-repellant textiles [20, 21], oleophobic surfaces [22], MEMS devices such as digital mirror devices [23, 24], and even for improving the performance of aircraft in rain [25, 26]. Typically, however, methods used to produce surfaces with extreme wetting behavior involve complicated and potentially expensive high-temperature/high-vacuum processes, temperature-sensitive materials, precise chemical synthesis, mechanical durability issues, and other factors that complicate the scalability and widespread implementation of these surfaces.

In this research, the surface wetting behavior of a variety of substrates, including titanium, glass, and polyethylene terephthalate (PET), have been modified by combinations of chemical and topographical modifications, with an aim at developing superhydrophilic and superhydrophobic surfaces on these materials. These modifications utilize combinations of established surface modification processes: sandblasting [15] and oxygen plasma treatments [27] for topography changes; very hydrophilic, nanoporous silica nanoparticle films [28]; and a low SFE fluorocarbon film [29]. While these methods have all been previously used to produce modified surface wetting behavior, they typically have not been used simultaneously. Although a myriad of methods for producing both superhydrophilic and superhydrophobic surfaces exist [30], the issue of surface wetting instability is generally present. Surface wetting instability refers to the tendency of a surface to degrade to normal hydrophilicity/hydrophobicity, due to surface contamination or other factors, and is a major difficulty related to the implementation of

superhydrophilic and superhydrophobic surfaces in applications. In addition to the wetting behavior, the effects of these surfaces on the optical properties of transparent substrates are of interest. With this in mind, the main objectives of this research are to develop simple methods of producing both superhydrophilic and superhydrophobic surfaces on a variety of materials by utilizing the synergistic effects of combinations of established surface modification processes; formally characterize the surface wetting stability of the surfaces created by these methods, which is frequently ignored in the literature, and delineate the effects of these fabrication processes on this stability; characterize these surfaces in terms of their surface wetting properties, surface morphology, surface elemental composition, and other relevant material properties; and identify limitations to producing extreme wetting behavior on any of the chosen substrate materials.

1.3 Organization of the Thesis

This thesis is divided into 5 chapters, with the present chapter introducing the relevant background on surface wetting physics and the motivation for this research. The current literature on the fabrication and implementation of superhydrophilic and superhydrophobic surfaces will be reviewed in chapter II. In chapter III, the fabrication methods and surface characterization techniques will be described, followed by the experimental results and discussion of these results in chapter IV. Finally, conclusions and recommendations for future work will be presented in chapter V.

II. LITERATURE REVIEW

2.1 Fabrication of Superhydrophilic and Superhydrophobic Surfaces

Owing to the fact that the SFE of a solid can be modified in a very general way through changes in surface topography and surface chemistry, a myriad of methods to fabricate superhydrophilic and superhydrophobic surfaces exist. The processes in these methods range from pure physical changes, to pure chemical changes, and frequently employ combined topography and chemistry changes. Nanoparticle films have been widely studied for use in fabricating extreme wetting/non-wetting surfaces, due to their ability to simultaneously change surface roughness and chemistry.

Nanoparticle films are often deposited via a sol-gel dip-coating process. The direct dip-coating method, in which a substrate is submerged in a colloidal nanoparticle solution, is simple and generally effective [31], but offers minimal control over film thickness and morphology. In the direct dip-coating method, film deposition is the result of physical adsorption or chemisorption [32] or, more rarely, self-assembly [33]. In contrast, the layer-by-layer (LbL) method, in which sequential multilayers of oppositely charged particles can be deposited from colloidal solutions through electrostatic interactions, provides unprecedented control of surface thickness and morphology [34]. A recent study by Lee *et al*. utilized the LbL method to produce superhydrophilic coatings consisting of alternating layers of SiO_2 and TiO_2 nanoparticles [35]. The LbL method allowed for control of film thickness through a linear relationship between film thickness and number of deposited SiO_2/TiO_2 bilayers, with an attendant increase in RMS surface roughness. However, this control came at the expense of fabrication simplicity, as 6 bilayers were required to produce superhydrophilicity. This equates to at least 24 submersions

per sample, as each bilayer required 4 submersions. In contrast, the direct dip-coating method often requires only a single submersion. The wetting behavior of nanoparticle films is not entirely due to pure surface chemistry or roughness changes, or even a combination thereof. For nanoparticle films, a third contribution becomes important: nanoporosity. A related study by Cebici *et al*., using the LbL technique to produce superhydrophilic surfaces using silica nanoparticles, established a critical number of SiO_2 layers required for superhydrophilicity [36]. In this study, it was hypothesized that the critical number of layers must correspond to a critical volume capacity of an interconnected porous network formed within the nanoparticle film, and the superhydrophilic behavior was enhanced by the "nanowicking" through this porous network.

The inclusion of TiO_2 in nanoparticle film assembly is due to the fact that TiO_2 exhibits superhydrophilic behavior under ultraviolet (UV) exposure, a phenomenon known as UV-induced or photo-induced hydrophilicity [37]. This behavior, combined with the photocatalytic properties of TiO_2, is of great interest for self-cleaning surfaces [38]. However, this wetting behavior rapidly diminishes once the UV illumination is removed, which severely limits its applicability. Permpoon *et al*. found that the duration of superhydrophilic behavior could be increased after the removal of UV illumination by the addition of 40 mol% of SiO_2 to the titania films, owing to the natural hydrophilicity of silica [39]. The freshly prepared films remained superhydrophilic for roughly four weeks, at which point the wettability degraded. Superhydrophilic behavior could be recovered by subsequent UV illumination, but the duration of superhydrophilic persistence diminished to roughly 3 weeks after this treatment.

Superhydrophilic and superhydrophobic surfaces that exist in nature provide ample inspiration for the fabrication of innovative surface features that affect surface wettability. This includes efforts to produce artificial surfaces that mimic the wetting behavior of the Stenocara beetle [40], the Namib Desert beetle [41], and raspberries [42, 43]. The most famous example is the so-called lotus effect [44], which has been extensively studied. The hydrophobic behavior of the natural waxy coating of the lotus leaf is enhanced by the presence of hierarchal micro- and nanostructures on the surface of the leaves. Saison *et al*. utilized nanoimprint lithography to recreate the biomimetic features of the lotus leaf and the *Papilionae Ulysse* butterfly wing, which also displays hydrophobic behavior, on methyltriethoxysilane (MTEOS) thin films [45]. The addition of these biologically-inspired topographies on MTEOS films resulted in an increase in WCA from 86° to 123° and 122° for the replicated lotus leaf and butterfly wing topographies, respectively.

Additionally, there is much interest in the ability to tune the wetting behavior of a solid, as well as to control the transition between wetting states. Rao *et al*. used surface functionalization with silanols to produce and control the hydrophobic behavior of silica films [46]. Silylation was achieved by immersing the silica films in a solution of various vol% of dimethylchlorosilane (DMCS) in hexane, and it was found that silica films treated with 6% and 12% DMCS were hydrophobic with WCAs of 115° and 136°, respectively, compared to 78° when treated with hexane alone. These hydrophobic silica films are thermally stable up to 295 °C, at which point the surface methyl groups oxidize into high-energy hydroxyl groups, resulting in hydrophilic or superhydrophilic behavior. Furthermore, Han *et al*. utilized a gradient UV-ozone treatment on a SAM-modified LbL silica nanoparticle film to visualize the striking

transition between wetting states [47]. This procedure resulted in a surface wetting gradient over a 40 mm length that exhibited a continuous, smooth transition from superhydrophobicity, to hydrophobicity, to hydrophilicity, to superhydrophilicity. The superhydrophobic region was dominated by the effects of a very low SFE SAM, while the superhydrophilic region was dominated by surface topography, most notably the nanoporosity of the silica film. This specifically demonstrated the rather delicate interplay between surface topography and surface chemistry on surface wetting behavior.

This delicate balance between surface topography and surface chemistry can be exploited to modify naturally hydrophilic materials to a superhydrophobic state simply through topography changes [48, 49]. Zhou *et al*. fabricated amorphous carbon thin films via rf-magnetron sputtering, and found that the surface morphology changed drastically as the substrate temperature was increased during deposition from room temperature to 400 °C [50]. At room temperature, the surface morphology of the carbon film was flat and smooth. As the substrate temperature increased, the surface roughness increased and carbon microstructures began to evolve until, at 400 °C, needle-like structures began to form. The room temperature carbon film was hydrophilic, with a WCA of 40°. However, as the surface roughness increased, the WCA dramatically increased, with the surface becoming truly hydrophobic through pure topography changes. The 400 °C carbon film was even superhydrophobic, with a WCA of 152°. Similarly, Guo *et al*. used a unique sandblasting procedure to create superhydrophobic titanium, which is naturally hydrophilic, through pure topography changes [51]. The titanium was sandblasted with glass micro-beads, which became embedded in the substrate. Hydrofluoric acid was then used to etch away the glass beads, which left a porous and cratered surface that was superhydrophobic.

Both of these cases are direct evidence of Cassie-Baxter wetting behavior, and are indicative of the potential effectiveness of pure surface topography modifications to drastically change the surface wetting behavior of a material.

Since the entire concept of surface wetting depends on the interactions of a solid and a liquid, surface contamination due to the liquid and atmosphere is a major issue [52]. This contamination alters the surface chemistry of the solid, and as such, is a major contributor to surface wetting instability. Development of surfaces with extreme wetting properties that are also absolutely stable is extraordinarily difficult, and the issue of surface wetting stability is often ignored in the literature. Mirshekari *et al*. investigated the effects of the atomic composition of co-sputtered $Ti_xSi_{1-x}O_2$ films on the surface wetting stability after the removal of UV illumination [53]. The results indicate that the optimum composition is $Ti_{0.6}Si_{0.4}O_2$, which remains superhydrophilic in excess of 50 h after the removal of UV illumination. Compared to pure TiO_2 films, which lost their superhydrophilic behavior within an hour, and pure SiO_2 films, which were only hydrophilic (WCA = 12°), this represents a major improvement in the superhydrophilic stability of these co-sputtered films.

For nanoparticle films, the surface wetting stability can depend on the specific chemistry of the sol-gel used as the source material. To this end, Ganjoo *et al*. compared the surface wetting behavior of silica nanoparticle films from two different tetraethylorthosilicate (TEOS) sol-gel formulations: a "low water" sol-gel with a H_2O/TEOS molar ratio of 0.34 and a "high water" formulation with a H_2O/TEOS molar ratio of 11.7 [54]. Surprisingly, the high water formulation produced WCAs in excess of 60°, due to a high amount of adsorbed water on the

silica surface. In contrast the low water formulation produced superhydrophilic silica films, with a reported stability in excess of 6 months. However, their stability claims are based on 6 measurements over the entire 6 month period, which is far too few to claim absolute stability since it does not consider the effects of surface contamination that can occur during frequent wetting/dewetting cycles. Nevertheless, this study highlights the marked effect that surface chemistry can have not only on surface wetting behavior, but also surface wetting stability.

2.2 Applications of Superhydrophilic and Superhydrophobic Surfaces

The impetus for the development of materials with superhydrophilic and superhydrophobic properties is for use in practical applications. Most of these applications are in the area of self-cleaning surfaces, usually with an emphasis on transparent materials [28, 55, 56]. Dhere *et al.* reported a method of producing transparent water-repellent silica films through a sol-gel process [57]. Recognizing that hydrophobic surfaces required a low sliding angle [58], i.e., the angle at which a substrate must be tilted in order for a liquid droplet on a surface to roll off under the force of gravity, to facilitate self-cleaning behavior, a silica film was modified with isobutyltrimethoxysilane (iso-BTMS) to produce a very hydrophobic (WCA ~ 140°) film with a sliding angle of 16°. In addition, the iso-BTMS modified silica film showed increased optical transmittance to 86%, compared to 75% for the untreated film. This type of simultaneously improved surface wetting and optical transmittance functionality is quite common.

Self-cleaning behavior can also be realized with superhydrophilic surfaces, though these approaches often attempt to utilize the photocatalytic properties of TiO_2 [59]. Liu *et al*. used a sol-gel process to develop SiO_2/TiO_2 bilayer films that were both self-cleaning and antireflective

[60]. However, the claimed self-cleaning behavior of these films is more closely related to photocatalytic properties of TiO_2, rather than the superhydrophilicity that is simultaneously induced during the UV illumination. In terms of optical properties, this surface coating on glass substrates produced a maximum optical transmittance of nearly 97%, which is a notable improvement over the optical transmittance of bare glass, which is in the range of 90-92%. However, due to the inherent stability issues of TiO_2-based superhydrophilic films, the lack of a formal stability analysis is a major limitation of this study.

In addition to self-cleaning applications, anti-fogging surfaces are of interest for practical use. Asthana *et al*. developed a hydrophilic surface coating for use on optical lenses [12]. The active element in the surface coating was Tiron, which has a molecular structure consisting of a benzene ring surface terminated with high-SFE hydroxyl and sulfonate groups. In order to promote good surface adhesion of the coating on the lenses, the coating was deposited with an organic-inorganic sol-gel technique, in which silica and titania nanoparticles were mixed with the Tiron before deposition. The addition of these inorganic components increased the surface adhesion of the coating through the formation of Si-O and Si-O-C bonds between the organic and inorganic components of the coating. When this coating was applied to an indium-tin-oxide coated optical lens, anti-fogging behavior was observed due to a decrease in WCA from 80° to 12.5°.

Modification of surface wetting behavior is also of interest for developing functional textiles. Chen *et al*. used silica nanoparticles to modify wool fibers to a superhydrophilic state [61]. Wool is naturally hydrophobic due to a natural coating of fatty acids, and this

hydrophobicity results in the need for wool fabrics to be dry-cleaned. The results show that the attachment of silica particles to wool fibers is based on electrostatic interactions. In addition, the superhydrophilicity greatly enhanced the washing fastness of wool fabrics in water, although durability concerns exist. Daoud *et al*. used a silica nanoparticle film functionalized with low SFE hexadecyl groups to produce nearly-superhydrophobic cotton [20]. The modified cotton fabric exhibited a WCA of 141°, and therefore has application as a stain-resistant fabric. Based on WCA measurements, unmodified cotton is superhydrophilic, although a major contribution to this superhydrophilicity is the absorbent properties of cotton; such a contribution was not considered in the definition of WCA from surface energy considerations. Again, however, the surface wetting stability and coating durability is a concern.

One of the more unique applications for modified surface wetting is in the area of prosthetic dentistry. Rupp *et al*. developed a method of producing superhydrophilic titanium with sandblasting, acid etching, and a specialized storage procedure [15]. Sandblasting and acid etching, which are commonly used in prosthetic dentistry to incur surface roughness on dental implants, usually results in a hydrophobic titanium surface with a WCA of 140°. However, by rinsing these surfaces in an N_2 environment after etching and storing them in an isotonic NaCl solution until use to prevent surface contamination, superhydrophilic behavior is induced in the titanium. This superhydrophilicity is potentially beneficial for the osseointegration of dental implants, especially during the initial cell adhesion processes. However, while these surfaces may be beneficial in clinical applications, the strict storage requirements may prevent more widespread use. If surface coatings, rather than simple roughness, are used to modify the wetting behavior, then additional mechanical benefits may be realized. Aksakal and Hanyaloglu

measured the bonding strength and hardness of several bio-compatible ceramics on titanium orthopedic implants, motivated by the fact that, in general, the interfacial bonding between metal and bone is low [62]. Thus, failure is prone to occur at the tissue-implant interface, and this limitation can be corrected by applying a surface coating to the implant that mutually adheres to both metal and bone. For dental applications, Bieniaś *et al*. determined that an intermediate SiO_2 coating results in a larger bond strength between dental implants and dental porcelain in prosthetic applications [63].

Due to the broad range of potential applications of both superhydrophilic and superhydrophobic surfaces, there is a need for a deeper understanding of not only how to fabricate such surfaces using simple methods, but also how specific surface properties, such as morphology, roughness, and surface chemistry, affect the surface wetting and stability. This work addresses this need by detailing simple methods to substantially modify the natural wetting properties of a variety of materials. In addition, the effects of each processing step on the modified surface wetting behavior are considered, these processing steps are correlated with surface properties that are necessary to produce superhydrophilic or superhydrophobic behavior, and specific limitations to producing extreme wetting behavior on certain substrates are identified.

III. EXPERIMENTAL METHODS

A variety of surface modifications have been employed to modify the natural surface wettability of Ti, glass, and PET. These modifications include sandblasting, surface cleaning, oxygen plasma treatments, silica nanoparticle films, a low SFE fluorocarbon film, and combinations thereof. The properties of these modified surfaces have been characterize by water contact angle measurements to quantify surface wetting properties, scanning electron microscopy for detailed surface morphology, energy dispersive X-ray spectroscopy (EDX) and X-ray photoelectron spectroscopy (XPS) for surface elemental composition, X-ray diffraction (XRD) for crystallographic information, surface profilometry for surface roughness measurements and silica nanoparticle film thickness measurements, and optical transmittance measurements on the transparent substrates.

3.1 Fabrication Processes

3.1.1 Substrate Materials, Sandblasting, and Cleaning

Ground-finish, grade 5 titanium plate (Ti6Al4V alloy, McMaster-Carr), soda-lime glass microscope slides (Ted Pella), and polyethylene terephthalate (PET) sheets (McMaster-Carr) were used as substrate materials. Titanium was chosen due to its widespread use in a variety of diverse applications, including automotive, aerospace, structural, and biomedical fields. Glass was chosen due to its ubiquitous nature as the most common optically transparent material. Likewise, PET is a commonly used plastic, especially for food packaging and biomedical applications; in addition, although it is not commonly used for optical applications, PET was chosen for its transparency to be used as a second optically transparent material for studying the optical properties of the silica nanoparticle films. Together, these substrates represent a variety

of material classes, namely metals, ceramics, and polymers. The Ti plate was machined into 3/4"×3/4" samples, while the PET sheets were cut with scissors into approximately 1"×1" samples; the glass slides were used as received. Titanium and glass samples were sandblasted with 165-μm alumina particles (Trin-blast 80, Trinity Tool Co.) in a commercial cabinet sandblaster (Trinity Tool Co.) for 10 s at a pressure of 240 kPa at normal incidence to generate bulk surface roughness. Since surface wetting behavior is so dependent on surface chemistry, after sandblasting, all samples (both sandblasted and bare) were cleaned with organic solvents to remove surface contamination. The Ti and glass samples were cleaned by sonication in acetone for 20 mins, followed by sonication in isopropyl alcohol for 20 min, and finally rinsed with deionized water and blown dry with nitrogen. PET samples were cleaned by the same process, except the acetone step was omitted to prevent crazing due to acetone uptake by the polymer.

3.1.2 Oxygen Plasma Treatments on Transparent Substrates

The sandblasting process produces microscale topography. If the optical properties of the substrate are of interest, sandblasting cannot be used because of undesirable light scattering due to the microscale topography created. For this reason, oxygen plasma treatments were used on the transparent substrate materials to create much smaller scale topography and preserve the optical transmittance of glass and PET. Oxygen plasma treatments are known to produce hydrophilic behavior in materials due to the creation of high-energy oxygen-containing functional groups on the material surface [64]. However, these functional groups are unstable, and the hydrophilic enhancement disappears quickly, sometimes within hours. Instead, the real benefit of this plasma treatment is to increase the sample surface energy to provide more energetically favorable conditions for silica nanoparticle film adhesion. For PET substrates,

oxygen plasma treatments are necessary for nanoparticle film deposition, as no nanoparticles will attach to untreated PET.

The plasma treatments on both glass and PET were performed with a reactive ion etcher (RIE) (PlasmaTherm SLR Series, Surface Technology Systems). In a conventional RIE, the specimen is placed between 2 electrodes that are biased by a voltage to produce a radio frequency (rf) electric field. Gas (oxygen in this study) is then introduced to the chamber and is ionized by the electric field; these ions bombard the specimen surface to produce the desired etching, sputtering, or surface excitation effects. The glass and PET samples were treated with an oxygen plasma with a power of 200 W and duration of 5 minutes. The oxygen flow rate and chamber pressure were 20 sccm and 100 mTorr, respectively. A photograph of the RIE used in this study is provided in Figure 4.

Figure 4: The PlasmaTherm SLR RIE used for oxygen plasma treatments.

3.1.3 Silica Nanoparticle Film Deposition

Silica nanoparticle films were deposited using a direct dip-coating method. SNOWTEX ST-PS-M colloidal string-of-pearls silica nanoparticle dispersion (Nissan Chemical) was used to produce silica nanoparticle solutions of 10%, 5%, and 2.5%, by weight. The as-received SNOWTEX consists of 12-25 nm diameter spherical silica nanoparticles arranged in chains of 4 (hence the designation "string-of-pearls") dispersed in water, with a concentration of 20%, by weight. The as-received solution was diluted with an appropriate mass of deionized water to produce the desired concentration. Silica nanoparticle films were deposited on the Ti samples using the 10% concentration solution only. Since the thickness of the nanoparticle film is heavily dependent on the solution concentration, silica nanoparticle films were deposited on the glass and PET substrates using the 5% and 2.5% solutions, so as to produce thinner nanoparticle films for optical purposes.

The films were deposited using an instrumented dip-coater (KSV DC, KSV Instruments), as seen in Figure 5. The motion of the dip-coater column was controlled with a stepper motor and proprietary software. The sample was secured with the clip on the dipping column, and then submerged into a beaker containing the nanoparticle solution using immersion and withdrawal speeds of 80 mm/min and an immersion time of 20 s. After dip-coating, the samples were heated on a 200 °C hotplate for 2 min to remove most of the moisture from the silica films. Additionally, the Ti and glass samples were annealed in a furnace at 500 °C in air for 5 min to ensure complete moisture removal; the low melting temperature of PET precluded this high temperature process from being used on the PET samples. The annealing temperature was

chosen to be below the sintering temperature of silica to prevent densification of the nanoparticle film, which is undesirable due to the role that porosity can contribute to superhydrophilicity.

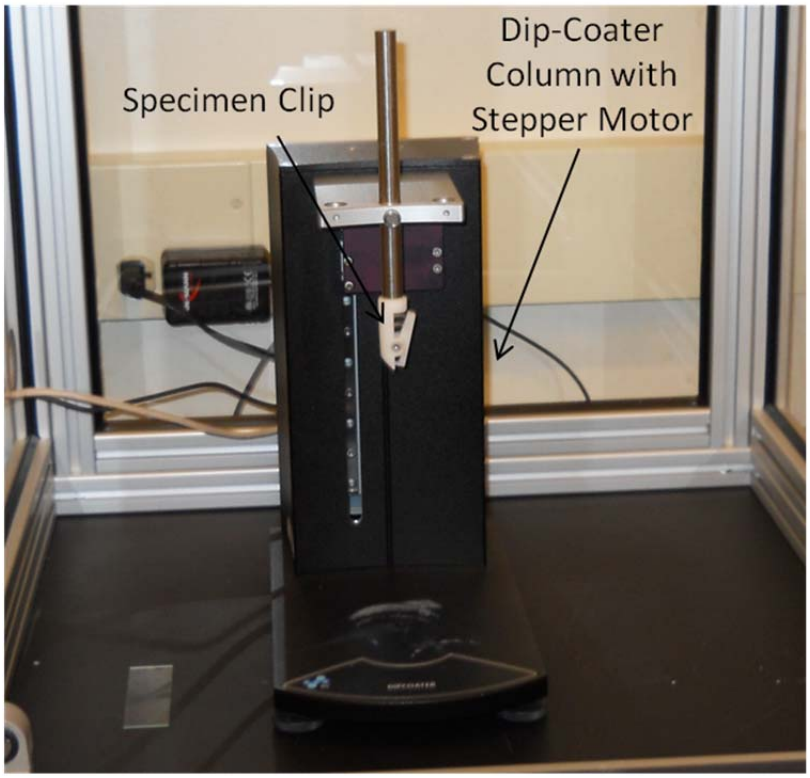

Figure 5: Dip-coater used to deposit silica nanoparticle films.

3.1.4 Low SFE Fluorocarbon Film Deposition

A low SFE fluorocarbon film used to promote hydrophobicity was deposited using the passivation capabilities of a deep reactive ion etcher (DRIE) (Surface Technology Systems). The film is deposited with the passivation step of the standard Bosch process, in which C_4F_8 gas is introduced to the vacuum chamber and a several-nanometer-thick CF_x film condenses on the sample surface under the action of an inductively-couple plasma (ICP) driven by a 13.56 MHz power source [65]. For deposition of low SFE films, the C_4F_8 flow rate, chamber pressure, coil

power, and process duration were 85 sccm, 8 mTorr, 20 W, and 21 s, respectively. A photograph of the DRIE is shown in Figure 6.

Figure 6: The DRIE used for low SFE fluorocarbon film deposition.

3.1.5 Summary of Fabricated Surface Conditions

Surfaces with different combinations of the above surface processes were fabricated to determine the synergistic effects of these processes on the surface properties. Eight Ti surface conditions, 12 glass surface conditions, and 6 PET surface conditions were investigated. A complete list of all the combinations investigated is provided in Table 1.

Table 1: Inventory of All Surface Conditions Investigated

Titanium	Glass	PET
As received (AR)	AR	AR
Sandblasted (SB)	SB	O_2 Plasma Treated (OP)
AR + 10% SiO_2	AR + 5% SiO_2	OP + 5% SiO_2
AR + Low SFE Film (LSF)	AR + 2.5% SiO_2	OP + 2.5% SiO_2
AR + 10% SiO_2 + LSF	OP + 5% SiO_2	OP + 5% SiO_2 + LSF
SB + 10% SiO_2	OP + 2.5% SiO_2	OP + 2.5% SiO_2 + LSF
SB + LSF	AR + 5% SiO_2 + LSF	
SB + 10% SiO_2 + LSF	AR + 2.5% SiO_2 + LSF	
	OP + 5% SiO_2 + LSF	
	OP + 2.5% SiO_2 + LSF	
	SB + 5% SiO_2 + LSF	
	SB + 2.5% SiO_2 + LSF	

3.2 Surface Property Characterization

3.2.1 Water Contact Angle Measurements

Measurement of water contact angles can be accomplished with a contact angle goniometer. A typical goniometer consists of a device for dispensing accurately-controlled volumes of liquid, a stage for positioning of the specimen to be measured, and a camera and light source for imaging the shape of a liquid droplet on the sample surface. Contact angles can then be measured directly from these images.

In this study, water contact angles were measured using an OCA 15 Contact Angle Measuring System (Dataphysics Instruments GmbH), as shown in Figure 7. A sample is placed on the stage and manually raised until it contacts a deionized water droplet of well-controlled volume at the end of the syringe and separates the droplet from the syringe as the stage is lowered. An image of this droplet is taken with the optical camera, and the WCA is measured from this image using proprietary software by defining a baseline and fitting the silhouette of the droplet to an ellipse. The WCA is then numerically calculated as the angle between the baseline and the tangent line at the intersection of the baseline and fitted ellipse. 3 μL droplets were used for most measurements, except for the most hydrophobic surfaces, where separation of the water droplet from the syringe was difficult due to the hydrophobicity of the surface and moderate hydrophilicity of the syringe. For these surfaces, 6 μL droplets were used, as they were heavy enough to allow separation from the syringe under the force of gravity.

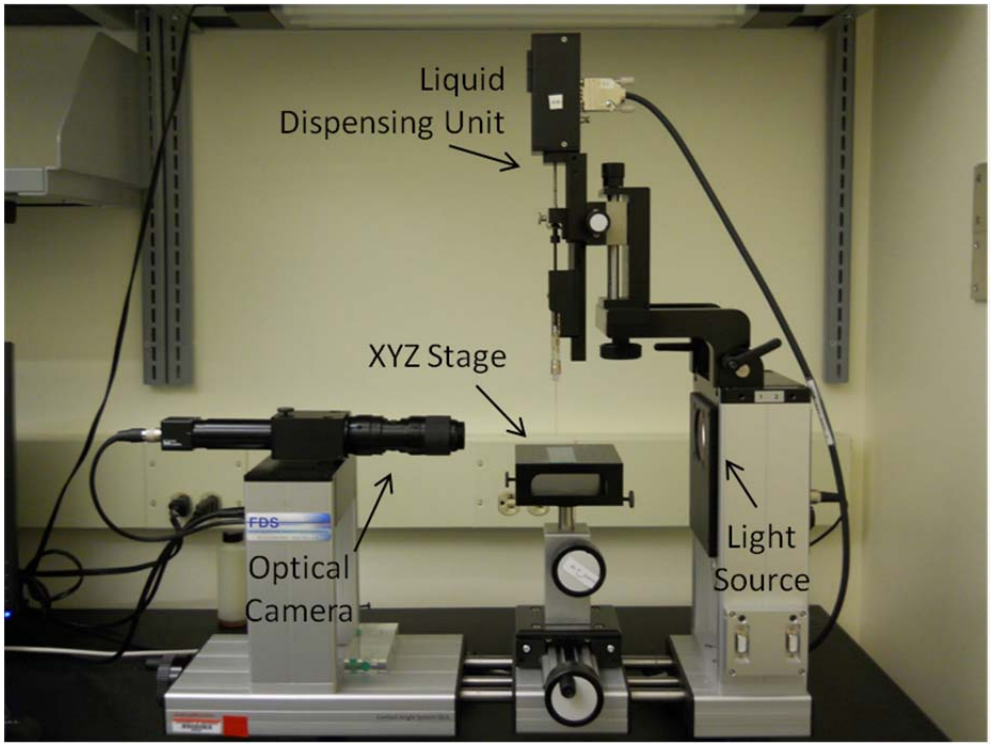

Figure 7: Contact angle goniometer used for WCA measurements.

3.2.2 Scanning Electron Microscopy

The scanning electron microscope (SEM) is specific type of electron microscope used for imaging surface features in vacuum with extremely high resolution, usually on the order of nanometers. A schematic of a typical SEM electron gun column is shown in Figure 8. A beam of electrons is produced with either a field emission or thermionic emission electron gun and is accelerated toward the specimen with a specified accelerating voltage. Focus and magnification of the beam is controlled with apertures and electromagnetic lenses. This incident electron beam interacts with the sample, causing secondary electrons from the sample and backscattered electrons from the incident beam to be emitted. As the beam is rastered over the specimen surface with the scan coil, the secondary electrons are collected by an electron detector which feeds a signal to a cathode ray tube, which then forms an image [66].

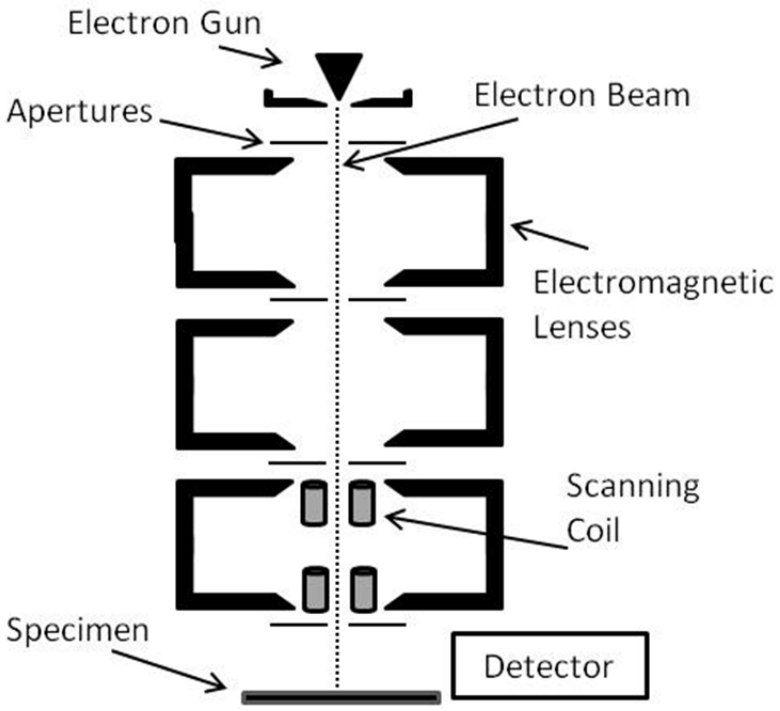

Figure 8: Schematic of a typical SEM beam column, showing the arrangement of the electron beam, electron gun, electromagnetic lenses, and scanning coil.

Generally, SEM requires conducting or semiconducting specimens to prevent undesirable surface charging that will cause electron beam deflections and a loss of image fidelity, as well as potential beam damage to polymer specimens. However, this requirement can be relaxed by sputter coating non-conductive specimens with a thin coating of a conducting material. Since neither the SiO_2 nanoparticles nor the glass substrates used in this study are conductive, sputter coating was employed to increase image quality. For imaging purposes, SiO_2 films on Ti were coated with tungsten, while all glass samples were coated with gold; the choice of material for these coatings was simply based on the sputtering target available on the date of imaging. Due to the combined effect of non-conductivity, beam damage, and low melting temperature, PET substrates were unable to be imaged by SEM due to immediate melting and ablation of the PET by the electron beam; this type of sample reaction can cause serious damage to the SEM hardware if the effused vapors condense on the exposed electron gun. Surface morphologies of the Ti and glass samples were imaged with an environmental SEM (ESEM) (Philips/FEI), as shown in Figure 9, operating in high vacuum mode with an accelerating voltage of 15 kV and a working distance of 10 mm.

3.2.3 Energy Dispersive X-ray Spectroscopy

The ESEM used in this study is equipped with an integrated energy dispersive X-ray spectrometer (EDX), which can provide elemental composition information. In addition to emission of secondary and backscattered electrons, interactions between the electron beam and the SEM specimen results in the excitation of bound electrons of the constituent elements in the specimen into higher energy states. As these excited electrons relax back to their ground states,

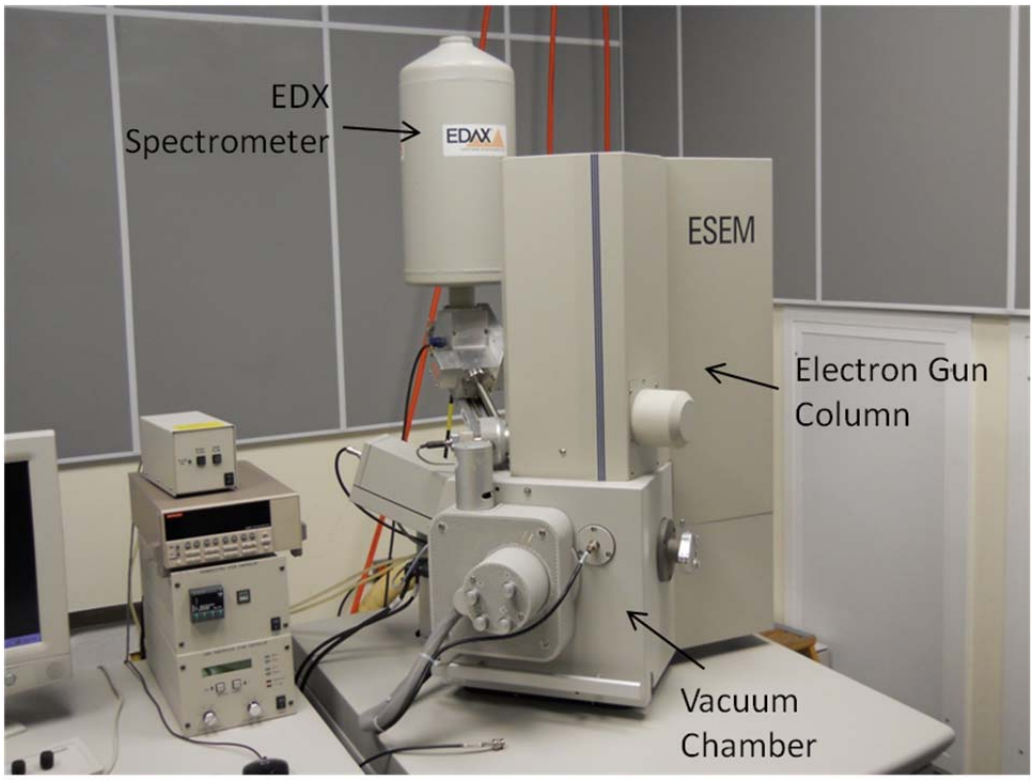

Figure 9: Photograph of the ESEM; the integrated EDX spectrometer can be seen behind the electron gun column.

they emit photons with energies that are characteristic of the elements in the specimen. Elements present in the specimen can be identified by the photon energy spectrum, measured by a Si (Li) detector. Since the photons are massless and have a neutral charge, they are able to easily escape from the material into vacuum, even if it was emitted from an atom in the bulk material below the sample surface. Therefore, EDX doesn't provide exclusive surface composition information, but rather the elemental composition of the sample down to the electron penetration depth, which can be several hundred nanometers deep [67]. EDX analysis of thin films will frequently detect substrate elements in the spectrum for this reason.

3.2.4 X-ray Photoelectron Spectroscopy

X-ray photoelectron spectroscopy (XPS, also called "electron spectroscopy for chemical analysis" [ESCA]) provides a method for explicitly analyzing the elemental composition and chemical states of a sample surface. In many ways, XPS can be considered the inverse process of EDX. The specimen is irradiated with a tightly-focused beam of X-ray photons with a specified energy, which interact with the sample. These photons have sufficient energy to overcome the electronic binding energy of the constituent elements of the sample and eject electrons from the material. The kinetic energy distribution of these ejected electrons are measured, and the binding energy of the electrons can be calculated as

$$E_{binding} = E_{photon} - (E_{kinetic} + \varphi) \tag{8}$$

where φ is the work function of the spectrometer. This binding energy is characteristic of the element and shell to which the electron belongs, and the elements present on the specimen surface can be identified with the measured binding energy spectrum. In contrast with EDX, due to the mass and charge of the ejected electrons, only electrons ejected from the top 1-10 nm of the specimen can escape to vacuum, and therefore XPS provides true surface elemental composition information. XPS requires an ultra high vacuum (UHV) environment to prevent interactions between the electrons and vacuum environment before reaching the detector.

XPS spectra were measured with a PHI VersaProbe (Physical Electronics, Inc.), which uses an Al anode to produce a monochromatic probe beam of Al K_α photons (ε = 1486 eV) and a hemispherical electron analyzer to measure ejected photoelectron energies. A schematic of a typical XPS beam setup and a photograph of the Versaprobe are shown in Figure 10.

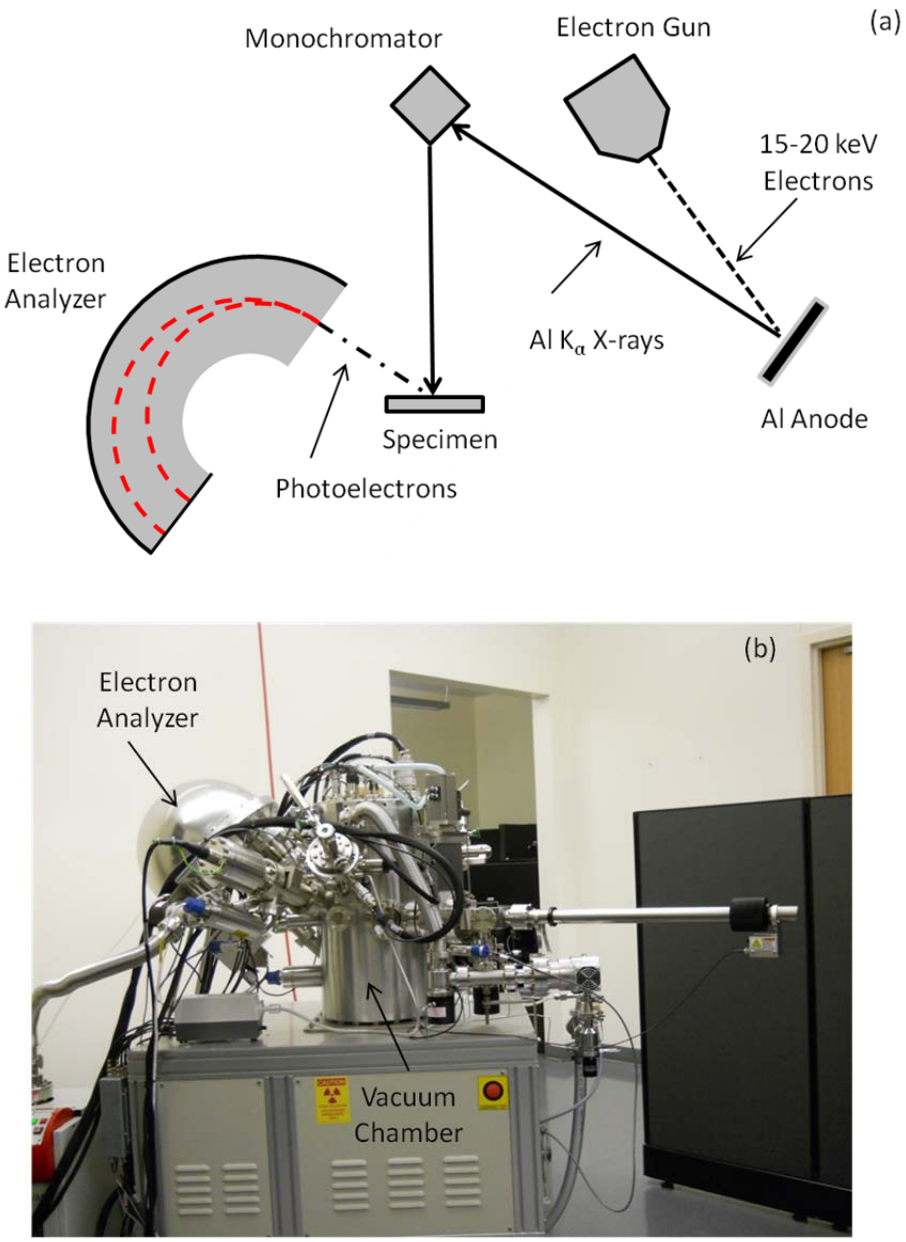

Figure 10: Schematic of a typical XPS beamline (a) and photograph of the VersaProbe XPS (b).

3.2.5 X-ray Diffraction

X-ray diffraction (XRD) is a technique for probing crystallographic information of a specimen based on constructive interference in the reflection of an incident collimated monochromatic X-ray beam. The governing equation of XRD is the Bragg equation [68]

$$n\lambda = 2d\sin\theta \tag{9}$$

where λ is wavelength of the X-ray, d is the distance between lattice planes in the specimen, θ is the angle between the incident X-ray beam and the specimen surface, and n is an integer. A schematic of Bragg diffraction is provided in Figure 11.

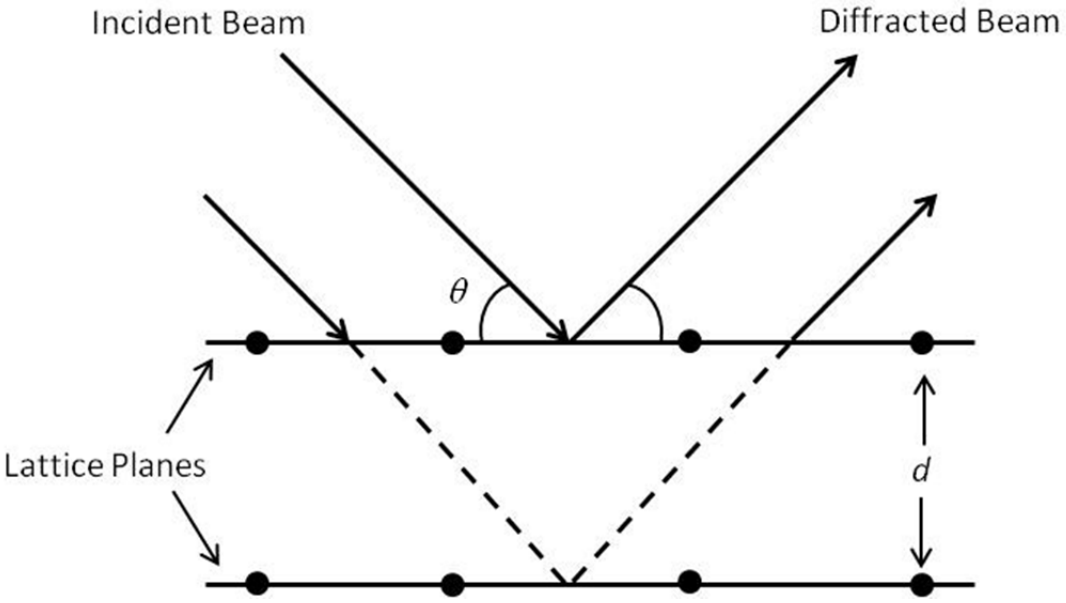

Figure 11: Illustration of Bragg diffraction by periodic lattice planes.

The path difference of the two X-rays in Figure 11 is $2d\sin\theta$, and constructive interference will occur in the reflections of the X-rays that satisfy the Bragg equation, resulting in a peak in the reflected intensity spectrum. This peak corresponds to a crystallographic plane for the specimen material. In this study, diffraction patterns of the Ti samples were measured with a Phillips XRD PW1830 operating in 2θ/ω mode, with a Cu K_α X-ray source (ε = 8028 eV).

For an infinitely large crystal, the diffraction peaks will be discrete lines. For "real" crystals with mosaic structures or polycrystalline materials with crystallites of finite extent, the

diffraction peaks are broadened [69]. The crystallite size can be estimated by the extent of this peak broadening through the Scherrer equation

$$X = \frac{0.9\lambda}{\Delta\theta \cos\theta} \tag{10}$$

where X is the crystallite size, λ is wavelength of the X-ray, θ is the Bragg angle, and $\Delta\theta$ is the full-width at half-maximum (FWHM) of the diffraction peak in 2θ space. In addition to peak broadening due to size effects, instrumental broadening can occur due to slight deviations in the energy spectrum of the monochromatic X-ray beam. The $\Delta\theta$ in the Scherrer equation must be corrected to account for this instrumental broadening, if the extent of the broadening is known. If not, then only qualitative, and no quantitative, information about the crystallite size may be obtained from the Scherrer equation by comparing the extent of peak broadening in a diffraction pattern.

3.2.6 Surface Contact Profilometry

Surface contact profilometry is a technique to measure the surface topography of a specimen by moving a diamond stylus with a well-defined tip radius of curvature over a surface, with a specified contact force. The tip radius of curvature is usually in the range of several micrometers, but can be as small as 10s of nanometers, while the contact force is typically in the milligram range. Contact profilometry can also be used to measure surface roughness parameters, such as average roughness (Ra), root-mean-square roughness (Rq), maximum peak-to-valley height (P-V), and others. In this study, the Ra and P-V surface roughness parameters of the modified Ti surfaces, as well as the silica film thicknesses on glass substrates, were measured

with a Dektak 3030 contact surface profilometer, with a 25 micron tip radius, a 3 mm scan length, and a 5 mg contact force.

3.2.7 Optical Transmittance Measurements on Transparent Substrates

The optical properties of materials can be experimentally measured with a spectrophotometer. A typical spectrophotometer measures transmittance by producing a reference beam of light with a well-defined wavelength (or, equivalently, frequency or photon energy, since these 3 quantities are related through the Planck-Einstein-de Broglie formulas [70]) and spectral intensity and measuring the intensity of the beam, usually with a photoresistor, after it passes through the specimen. A schematic of a spectrophotometer is shown in Figure 12.

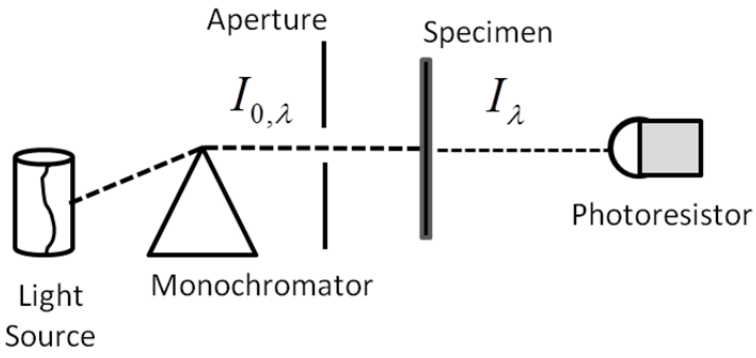

Figure 12: Schematic of a spectrophotometer, showing the reference beam intensity produced by the light source and monochromator and the measured beam intensity transmitted though the specimen.

The spectral transmittance is quantified in terms of the reference beam intensity as

$$\tau_\lambda = \frac{I_\lambda}{I_{0,\lambda}} \tag{11}$$

where τ_λ, I_λ, and $I_{0,\lambda}$ are the spectral transmittance, measured spectral intensity, and spectral intensity of the reference beam at a wavelength λ, respectively. A general radiative energy balance requires that

$$\tau_\lambda + \alpha_\lambda + \rho_\lambda = 1 \tag{12}$$

where α_λ and ρ_λ are the spectral absorbance and spectral reflectance of the material, respectively.

In general, a spectrophotometric measurement will not be able to completely specify all three optical properties of a material. However, for materials that are transparent at visible wavelengths, the analysis can be simplified by assuming that the spectral absorbance is negligibly small. For materials for which this assumption is valid, the spectral reflectance is simply

$$\rho_\lambda = 1 - \tau_\lambda \tag{13}$$

The basis for this assumption is that transparent materials are transparent because their bandgaps are substantially larger than the energies of visible-wavelength photons [71]. Since the energies of these photons are insufficient to excite valence electrons into the conduction band, the probability of absorption of these photons is negligibly small, and thus the absorbance is negligible. Transmittance spectra for the glass and PET samples were measured with a Cary 500 UV-vis-NIR spectrophotometer (Varian, Inc.) in a wavelength range of 200-800 nm, with a data resolution of 1 nm, spectral bandwidth of 2 nm, and baseline correction.

IV. RESULTS AND DISCUSSION

4.1 Titanium Surface Modifications

4.1.1 Surface Wettability

The average WCAs of the 8 titanium surface conditions listed in Table 1 were measured to determine the initial wettabilities of these surfaces. Three samples of each surface condition were measured, with 3 WCAs per sample, resulting in an average based upon 9 WCA measurements. The results are summarized in Figure 13, which shows optical images of representative surface wetting behavior, along with the average WCAs, for each surface condition. The sandblasting procedure results in a roughly 20° decrease in WCA (Figure 13 (e)) compared to AR Ti (Figure 13 (a)), demonstrating Wenzel-type wetting behavior. Superhydrophilic behavior is exhibited by both the AR + 10% SiO_2 (Figure 13 (b)) and SB + 10% SiO_2 surfaces (Figure 13 (f)), with the sandblasted variant being slightly more hydrophilic. The superhydrophilic nature of these surfaces is mediated by a change in surface chemistry to that of silica, which is a very hydrophilic material, as well as the small-scale roughness and capillary effects due to the inherent nanoporosity of the nanoparticle film. All surfaces with the low SFE fluorocarbon film show vastly improved hydrophobic properties compared to the non-passivated counterparts. However, only the SB + 10% SiO_2 + LSF surface (Figure 13 (h)) exhibits true superhydrophobic behavior, which is likely due to Cassie-Baxter wetting behavior. The SB + LSF surface condition is nearly superhydrophobic (Figure 13 (g)), which highlights the benefits of the bulk scale roughness created by the sandblasting procedure to creating superhydrophobic surfaces, especially compared to the wetting behavior of the AR + LSF (Figure 13 (c)) and AR + 10% SiO_2 + LSF (Figure 13 (d)) surfaces. Using these fabrication

methods, the fabrication of both superhydrophilic and superhydrophobic surfaces on Ti is demonstrated.

4.1.2 Surface Wetting Stability

In order to determine the surface wetting stability of the 8 Ti surface conditions, the average WCA of each condition was measured every 6 days for a period of 54 days. Again, averages were based upon 9 WCAs (3 measurements × 3 samples). Plots of average WCA over time are shown in Figure 14.

As can be seen, the SB + 10% SiO_2 and the AR + 10% SiO_2 surface modifications are highly stable, as the SB + 10% SiO_2 surface retains the superhydrophilic characteristics for 54 days, while the AR + 10% SiO_2 surface remains superhydrophilic for 36 days. Although a slight degradation in the surface wetting properties occurs over this time period, i.e., the average WCAs increase by roughly 5°, this is a vast improvement in stability over the AR and SB Ti surfaces, whose WCAs increase by roughly 20° and 40°, respectively, during the same time period. The SB + 10% SiO_2 + LSF surface modification produces an extremely stable superhydrophobic surface, with no surface wetting degradation during the entire 54 day period. The other hydrophobic surface modifications are slightly less stable, with a decrease in WCA of roughly 3-5°.

The origins of the stability of the superhydrophilic and superhydrophobic surfaces are due to different mechanisms. Instability is primarily due to organic surface contamination build-up [52] during surface wetting, so a surface with stable wetting behavior must be either

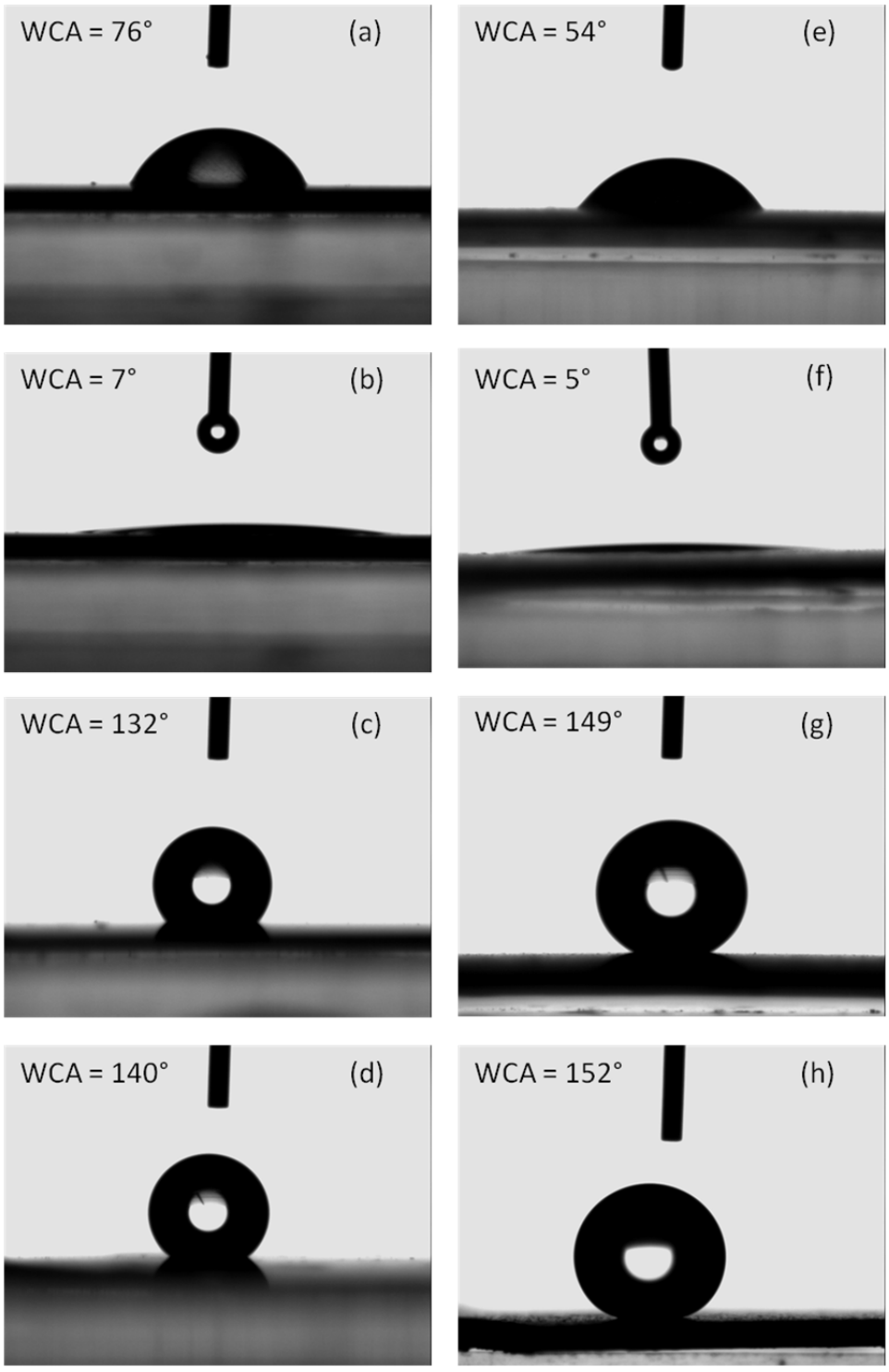

Figure 13: Optical images showing the initial wetting behavior of the AR (a), AR + 10% SiO_2 (b), AR + LSF (c), AR + 10% SiO_2 + LSF (d), SB (e), SB + 10% SiO_2 (f), SB + LSF (g), and SB + 10% SiO_2 + LSF (h) Ti surface conditions, along with average WCA values for each condition.

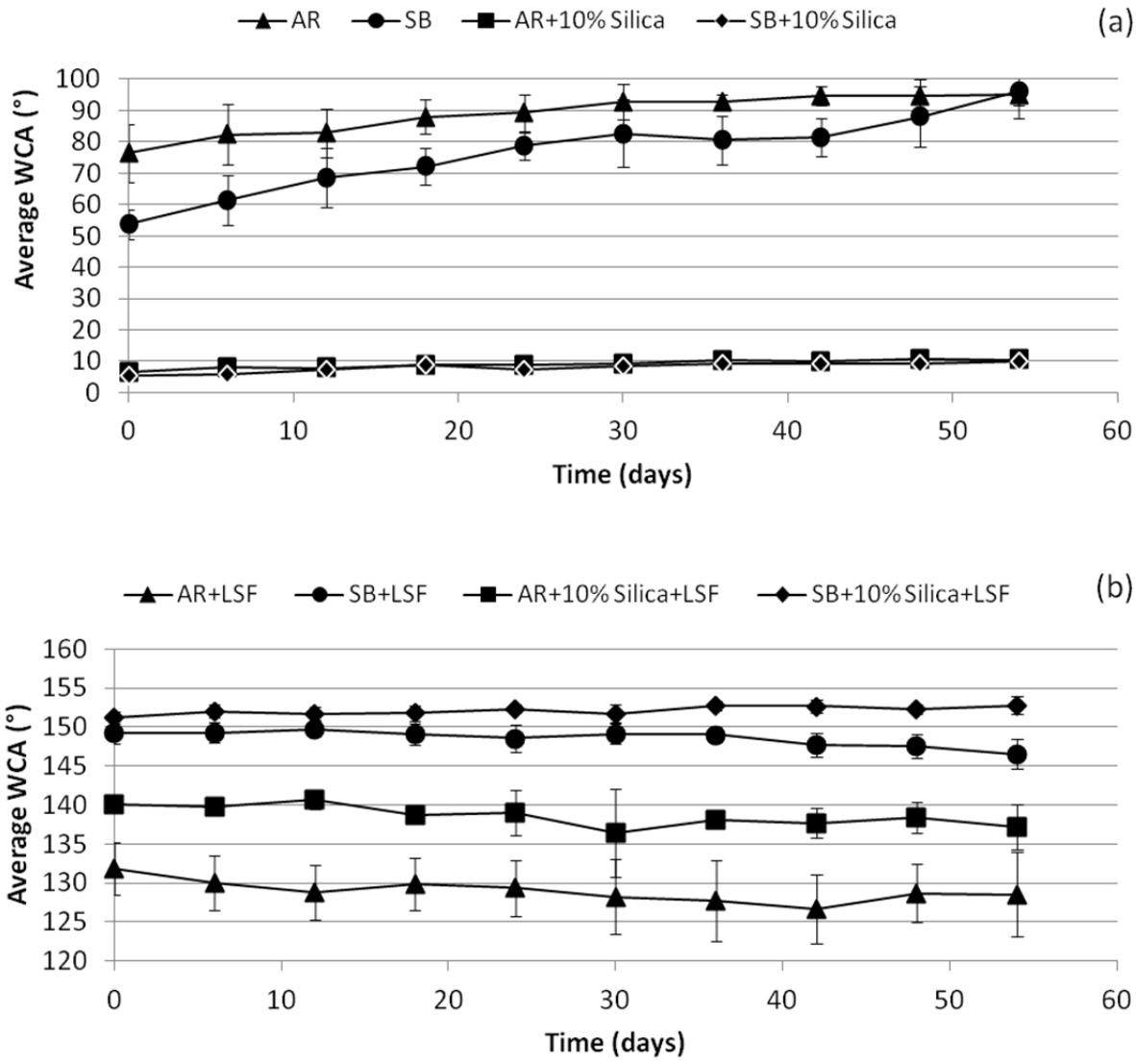

Figure 14: Average WCA of (a) the hydrophilic surfaces and (b) the hydrophobic surfaces over time. Error bars denote one standard deviation.

resistant to contamination or employ methods to remove contamination, such as photocatalysis. The stability of the fabricated superhydrophilic surfaces is highly dependent on the surface chemistry and structure of the silica nanoparticle film. The surfaces of the silica nanoparticles are terminated with silanol groups, which contain high-energy hydroxyl groups. These –OH groups help facilitate hydrophilicity via hydrogen bonding with adsorbed water [72]. Specifically, this affinity for water is higher than the affinity for organic surface contamination [39], resulting in a resistance, but not immunity, to surface contamination and an increase in stability. The nanoporous structure of the silica film contributes to the stability by increasing the number of active –OH groups from only those at the material surface to include those within the nanoporous network. For the method of silica nanoparticle deposition reported, the annealing temperature is a potential concern, since it is above the temperature at which silica begins to dehydroxylize. However, this type of surface dehydration is a non-equilibrium process, and significant dehydroxylation occurs over a period of hours to days, not minutes [72]. Furthermore, hydroxyl groups within the nanoporous silica network do not readily dehydrate, because of the increased packing of hydroxyl groups in the region between silica particles where the radius of curvature is negative [72]. Thus, the short annealing time insures that dehydration of hydroxyl groups is minimal and has a negligible effect on the surface wetting behavior. In contrast, the stability of the superhydrophobic surface is mostly due to the wetting behavior. Large WCAs correspond to small areas of solid-liquid interfacial area, and this non-wetting behavior results in a decrease in surface area available for contamination due to surface wetting.

4.1.3 Surface Morphology

The sandblasting and silica nanoparticle deposition processes produce vastly different surface morphologies compared to the AR Ti. SEM micrographs of the effects of these processes on surface morphology are shown in Figure 15. Since the dimensions of the low SFE film were below the resolution limit of the SEM, and since the film was likely beam-sensitive, those samples were not imaged.

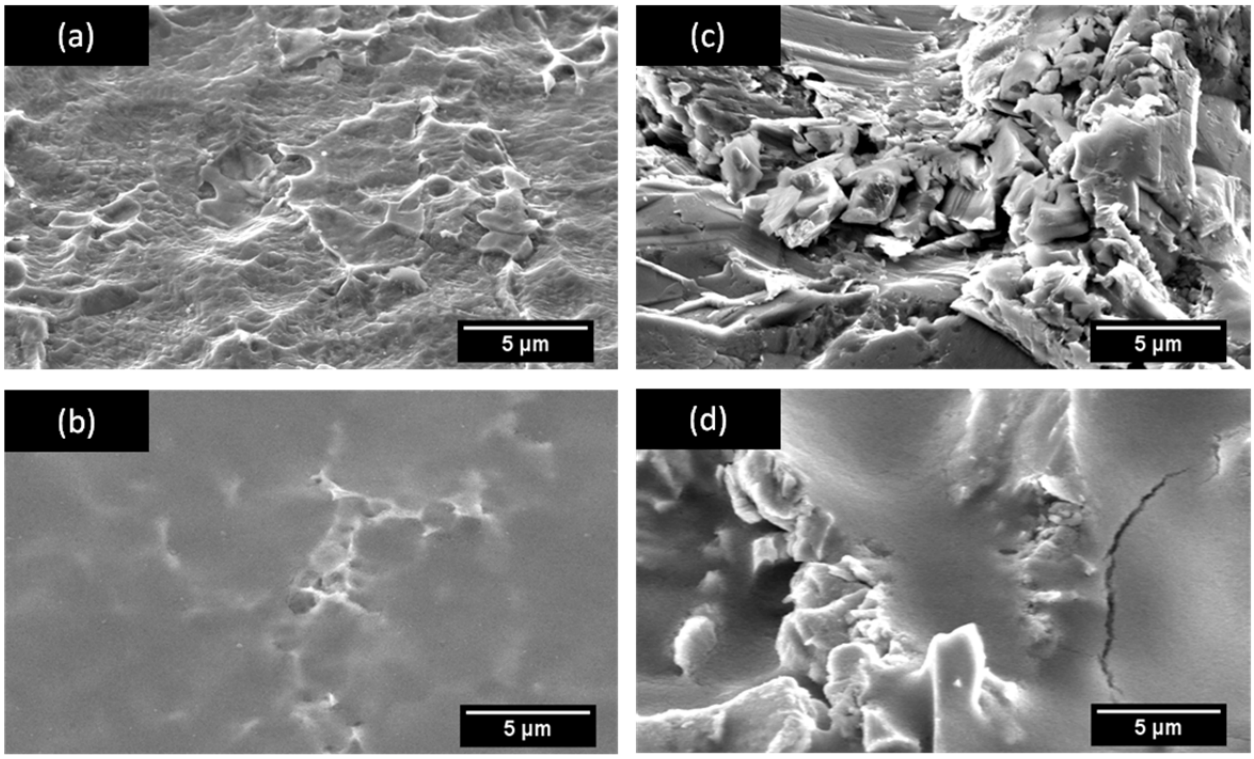

Figure 15: SEM micrographs of the AR (a), AR + 10% SiO_2 (b), SB (c), and SB + 10%SiO_2 (d) Ti surfaces, at 5,000× magnification and 45° incidence.

The AR surface consists of random, web-like surface features due to the manufactured ground surface finish. The addition of silica nanoparticles to this surface results in a conformal

coating with a much more uniform surface morphology. The sandblasting procedure has a much more marked effect on the surface morphology through significant surface damage, material rearrangement, and the formation of randomly-distributed micron-sized peaks, valleys, and craters in the Ti surface. Silica nanoparticle deposition on this surface again results in a continuous, conformal nanoparticle coating, with the micron-sized surface features from the sandblasting process being retained.

4.1.4 Surface Elemental Composition

EDX spectra for all 8 Ti surface conditions are shown in Figure 16. All samples show peaks corresponding to the constituent elements of grade 5 titanium: Ti, Al, and V. The spectra from the AR + 10% SiO_2, AR + 10% SiO2 + LSF, SB + 10% SiO_2, and SB + 10% SiO_2 + LSF contain large Si and O peaks, owing to the presence of the silica nanoparticle film. In addition, the AR + LSF, AR + 10% SiO_2 + LSF, SB + LSF, and SB + 10% SiO_2 + LSF spectra show slight F peaks, indicating the presence of a very thin fluorocarbon film. It should be noted that for all the sandblasted samples, the aluminum signature is far too prominent to be accounted for by the aluminum in the titanium alloy alone. This information, combined with the unexpectedly large oxygen peaks from the SB and SB + LSF samples, indicates that alumina fragments become embedded in the Ti alloy surface during the sandblasting procedure. In addition, anomalous nitrogen signatures appear in all samples without silica nanoparticle films due to the increased affinity for atmospheric nitrogen adsorption of titanium, compared to that of silica [73].

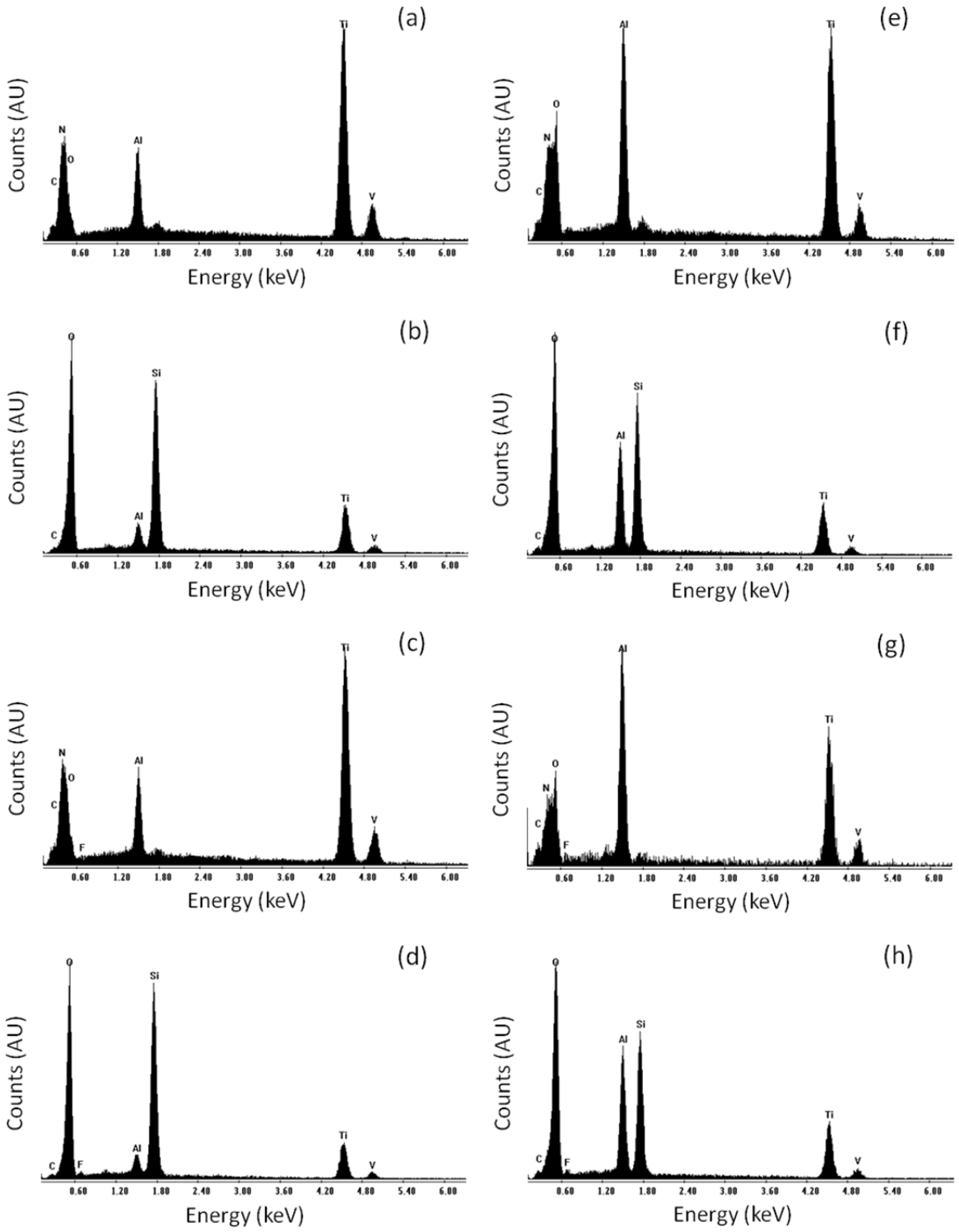

Figure 16: EDX spectra of the AR (a), AR + 10% SiO_2 (b), AR + LSF (c), AR + 10% SiO_2 + LSF (d), SB (e), SB + 10% SiO_2 (f), SB + LSF (g), and SB + 10% SiO_2 + LSF (h) Ti surface conditions.

XPS spectra of the AR, SB, SB + 10% SiO_2, and SB + 10% SiO_2 + LSF surfaces are shown in Figure 17. The AR surface spectrum shows high oxygen content, corresponding to the presence of a native oxide layer. Note the lack of peaks corresponding to Al and V, which had appeared in the EDX spectrum of the same surface condition; this indicates those elements are confined to the bulk of the Ti alloy, and not the surface. The SB spectrum exhibits Al peaks, as well as a much larger O signature than the AR sample, which is further evidence that alumina particles become embedded in the Ti surface during sandblasting. The spectrum of the SB + 10% SiO_2 surface condition is completely composed of Si and O peaks, with no Ti signature, which confirms that the silica nanoparticle film forms a completely continuous surface coating.

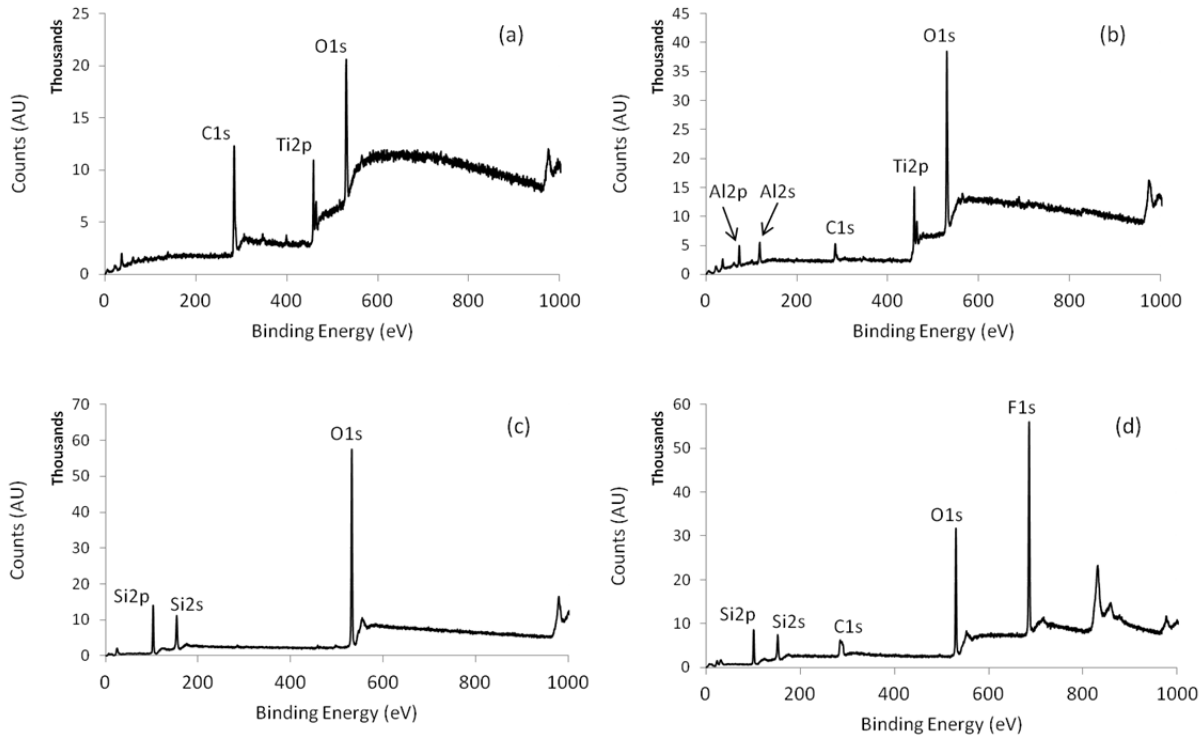

Figure 17: XPS spectra of the AR (a), SB (b), SB + 10% SiO_2 (c), and SB + 10% SiO_2 + LSF (d) Ti surface conditions.

Note also that the SB + 10% SiO_2 surface spectrum lacks a carbon signature, which was present in both the AR and SB spectra, which is evidence that the silica nanoparticle film may be resistant to organic surface contamination. Finally, the SB + 10% SiO_2 + LSF spectrum shows a very prominent F peak, along with an associated C peak, due to the low SFE fluorocarbon film. In addition, the presence of Si peaks in the spectrum indicates that the fluorocarbon film is only several nanometers thick.

4.1.5 XRD

XRD patterns of the AR Ti alloy, the SB Ti surface, and the silica nanoparticle film on an AR Ti substrate are shown in Figure 18. By comparing the AR and SB patterns, it is clear that the surface is not changed crystallographically by the sandblasting process, i.e., no new diffraction peaks appear, nor do existing peaks disappear. The main peaks in the patterns located at 38.5°, 40.5°, 53.3°, 63.6°, and 71.0° (in 2θ space), as well as several other less prominent peaks, correspond to the α-Ti phase, with the remainder corresponding to minor amounts of the β-Ti phase. However, peak broadening is also evident in the SB pattern, which can indicate a decrease in crystallite size or an increase in dislocation density induced by plastic deformation caused by the sandblasting process.

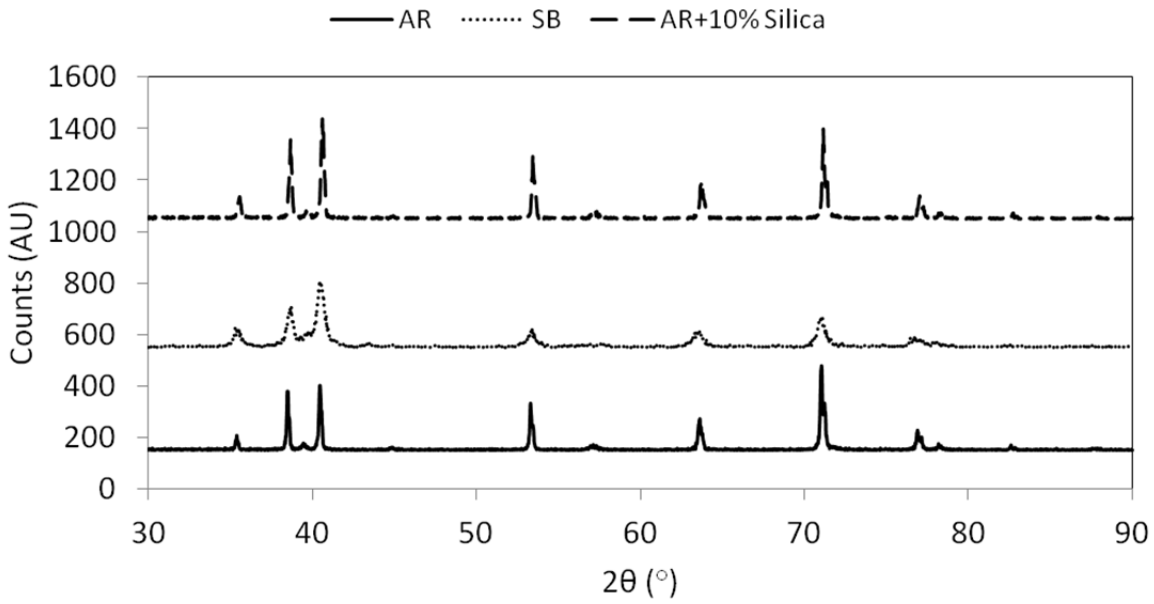

Figure 18: XRD patterns of the AR, SB, and AR + 10% SiO_2 surface conditions.

4.1.6 Surface Roughness Measurements

Average surface roughness (Ra) and maximum peak-to-valley height (P-V) surface roughness parameters were measured to quantify the surface roughness of the AR, SB, AR + 10% SiO_2, and SB + 10% SiO_2 surface conditions. Two samples per surface condition were measured, with 3 measurements per sample, resulting in average values based on 6 measurements. Bar graphs of the surface roughness parameter measurements are shown in Figure 19.

As expected, the sandblasting procedure produces a large increase in both Ra and P-V, while the silica nanoparticle film produces another slight increase in both parameters. From a surface wetting standpoint, surface roughness is vastly more important for creating superhydrophobic surfaces than superhydrophilic surfaces. Whereas both the AR + 10% SiO_2

and SB + 10% SiO_2 surfaces, which have vastly different surface roughnesses, were superhydrophilic due to capillary effects and nanoporosity, the most hydrophobic surfaces required the large-scale roughness afforded by the sandblasting procedure.

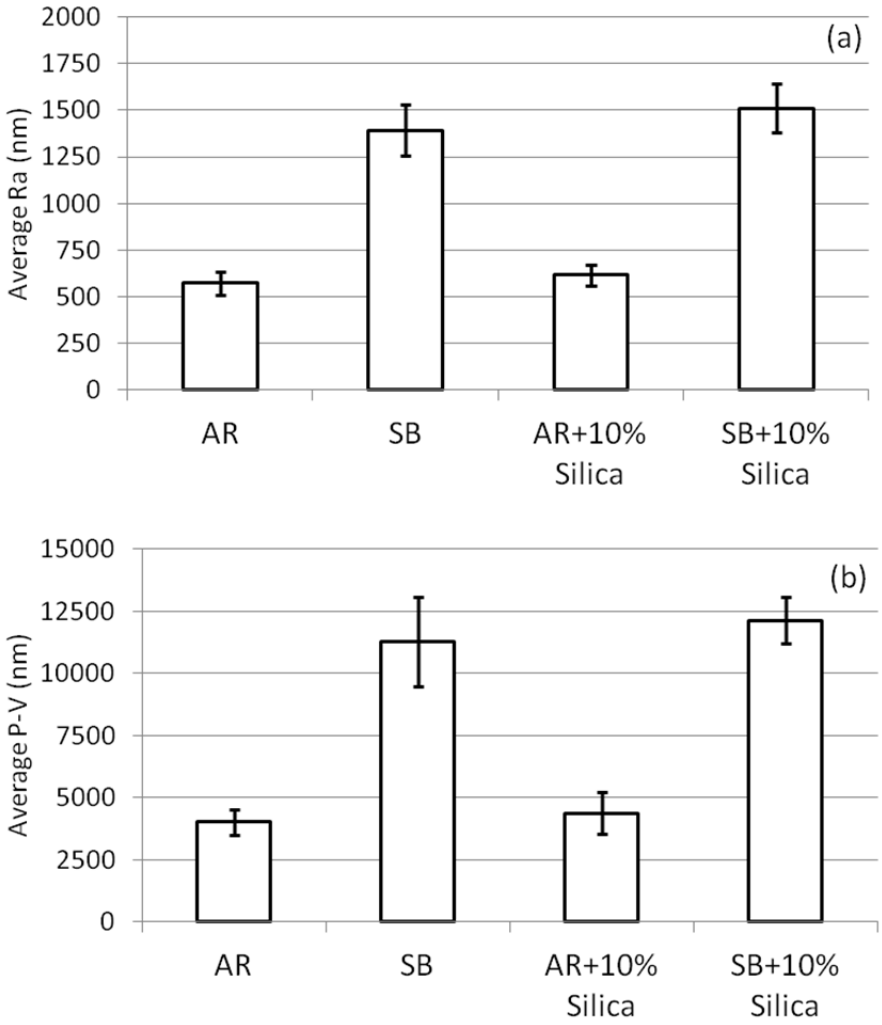

Figure 19: Average Ra (a) and P-V (b) surface roughness parameters of the AR, SB, AR + 10% SiO_2, and SB + 10% SiO_2 Ti surface conditions. Error bars denote one standard deviation.

The SB + LSF surface exhibited nearly superhydrophobic behavior, ostensibly due to the large P-V parameter which is favorable for inducing Cassie-Baxter wetting behavior. The

superhydrophobicity of the SB + 10% SiO_2 + LSF surface was mediated by adding nanoscale roughness from the silica nanoparticle film to the bulk scale roughness of the sandblasted surface to form a hierarchical roughness structure.

4.2 Glass Surface Modifications

4.2.1 Surface Wettability

The average WCAs of the 12 glass surface conditions listed in Table 1 were measured to determine the initial wettabilities of these surfaces. Three samples of each surface condition were measured, with 3 WCAs per sample, resulting in an average based upon 9 WCA measurements. The results of the hydrophilic and hydrophobic surfaces are summarized in Figures 20 and 21, respectively, which shows optical images of representative surface wetting behavior, along with the average WCAs, for each surface condition.

As can be seen in Figure 20, bare glass is nearly superhydrophilic on its own, due to the fact that silica is a naturally very hydrophilic material. Sandblasted glass is superhydrophilic due to Wenzel-type wetting behavior; however, the sandblasting process also severely impacts the transparency of glass, meaning that such a surface cannot be used for optical applications. Furthermore, initial superhydrophilic behavior is achieved with all surface conditions that incorporate silica nanoparticles. The initial wetting behavior of these 4 surfaces is relatively insensitive to both silica nanoparticle concentration and oxygen plasma treatments.

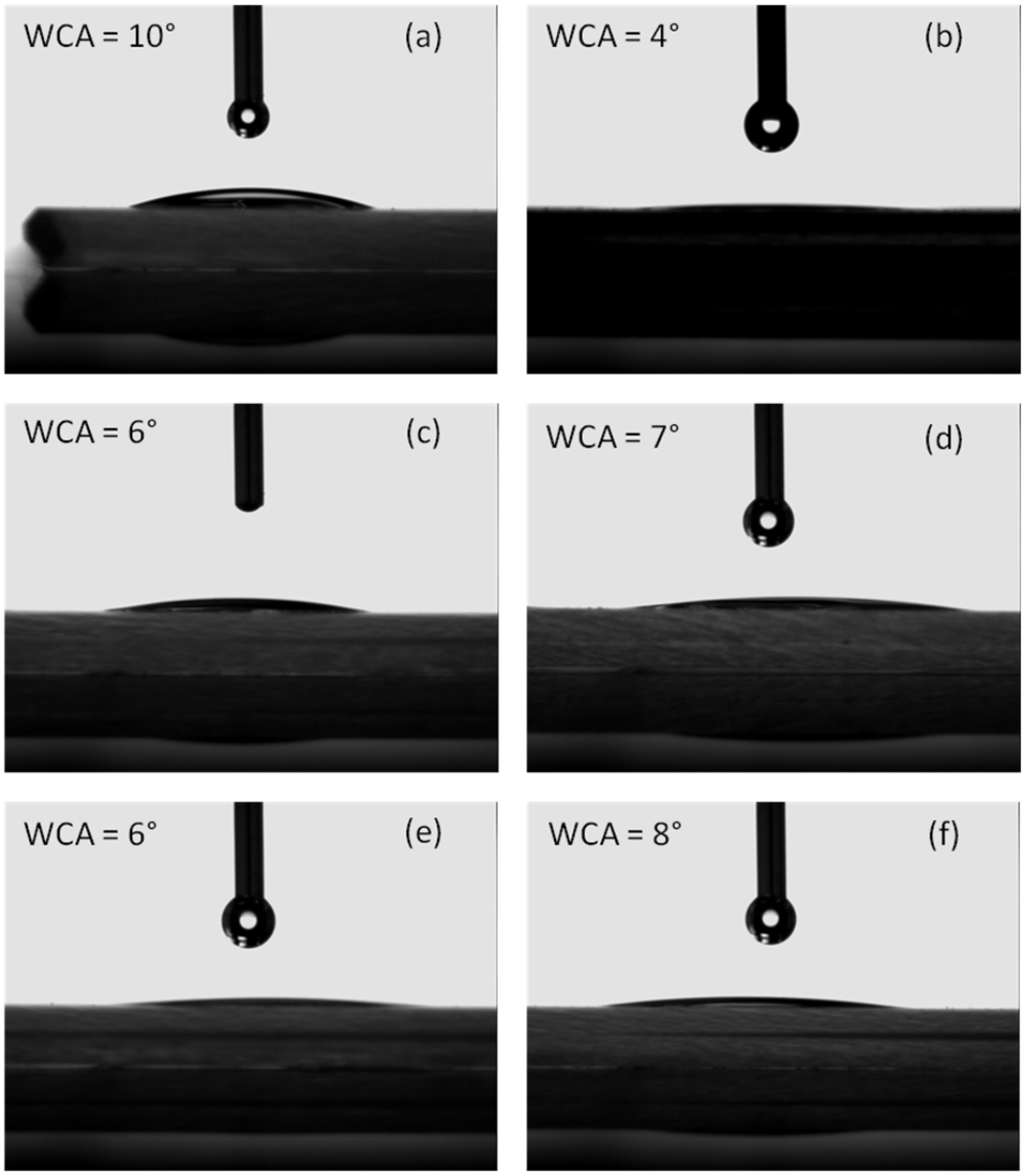

Figure 20: Optical images showing the initial wetting behavior of the AR (a), SB (b), AR + 5% SiO_2 (c), AR + 2.5% SiO_2 (d), OP + 5% SiO_2 (e), and OP + 2.5% SiO_2 (f) glass surface conditions, along with average WCA values for each condition.

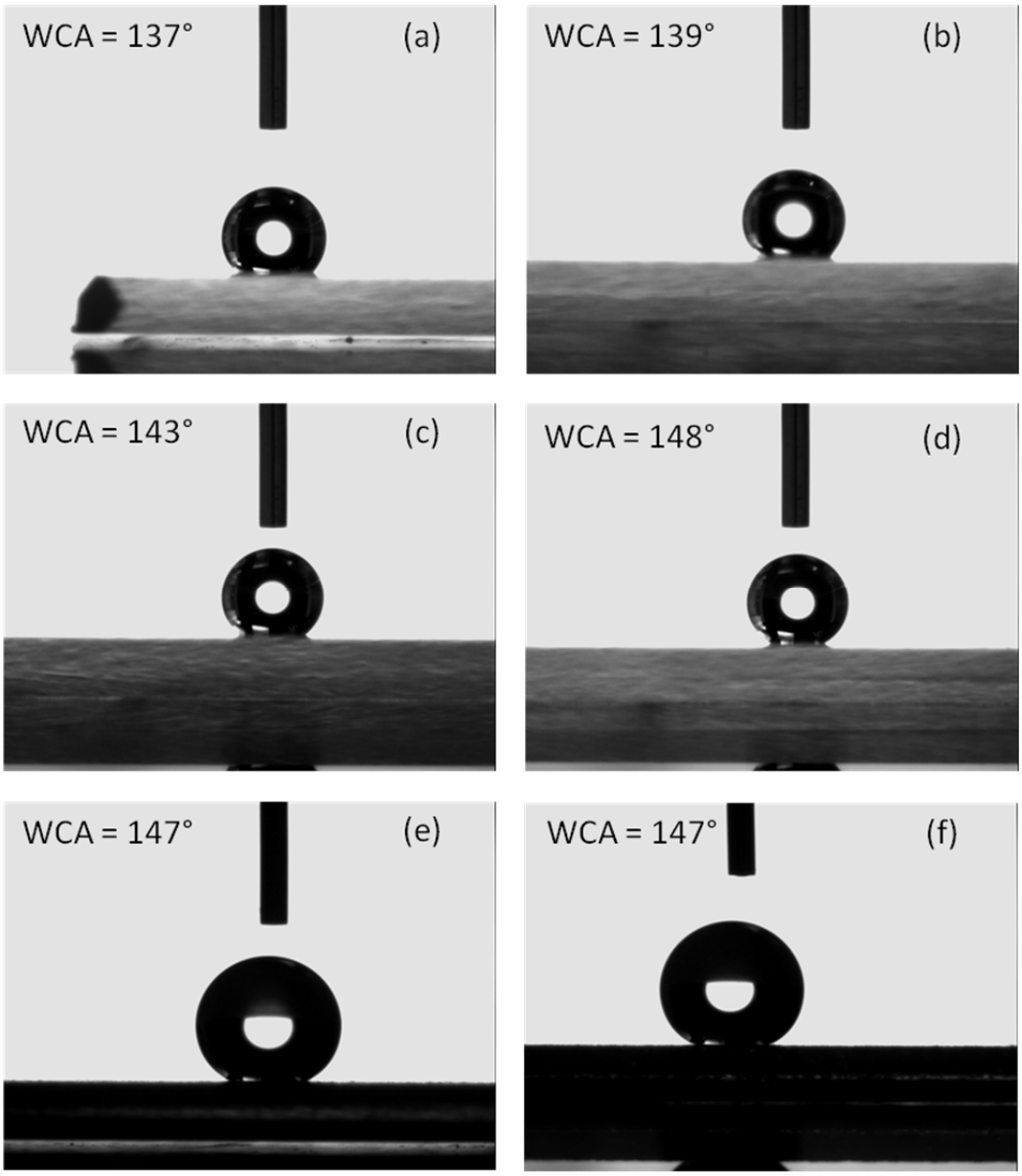

Figure 21: Optical images showing the initial wetting behavior of the AR + 5% SiO_2 + LSF (a), AR + 2.5% SiO_2 +LSF (b), OP + 5% SiO_2 +LSF (c), OP + 2.5% SiO_2 +LSF (d), SB + 5% SiO_2 +LSF (e), and SB + 2.5% SiO_2 +LSF (f) glass surface conditions, along with average WCA values for each condition.

In contrast with the Ti surface modifications, superhydrophobic behavior was not achieved for any surface modification on glass. Figure 21 shows that very hydrophobic behavior is exhibited by both 5% and 2.5% SiO_2 concentrations on bare glass, and that oxygen plasma treatments prior to nanoparticle deposition can slightly improve the hydrophobicity by roughly 6-9°. However, none of these surface conditions have sufficient surface roughness to induce true superhydrophobic behavior. Even the sandblasting procedure is insufficient to provide adequate surface roughness for superhydrophobic behavior, as both the SB + 5% SiO_2 + LSF and SB + 2.5% SiO_2 + LSF surfaces have average WCAs of 147°. This competition between surface roughness and optical properties is a major limitation for creating transparent superhydrophilic/superhydrophobic surfaces on glass.

4.2.2 Surface Wetting Stability

The surface wetting stability of the 12 glass surface conditions were measured over 24 days for the AR, AR + 5% SiO_2, AR + 2.5% SiO_2, OP + 5% SiO_2, and OP + 2.5% SiO_2 surfaces, and over 17 days for the SB, AR + 5% SiO_2 + LSF, AR + 2.5% SiO_2 + LSF, OP + 5% SiO_2 + LSF, OP + 2.5% SiO_2 + LSF, SB + 5% SiO_2 + LSF, and SB + 2.5% SiO_2 + LSF surfaces, as shown in Figure 22. Again, averages were based upon 9 WCAs (3 measurements × 3 samples).

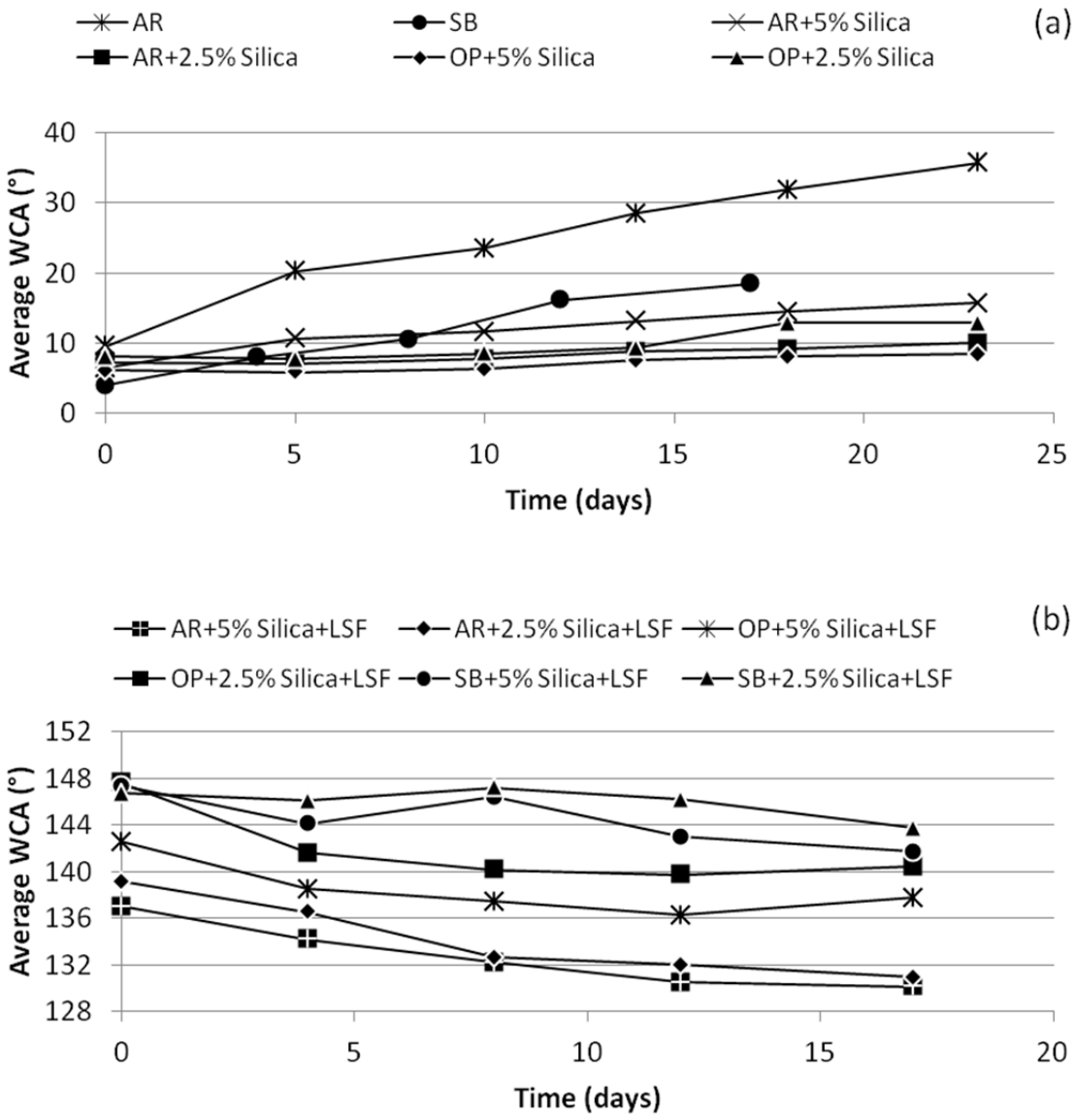

Figure 22: Average WCAs of (a) the hydrophilic surfaces and (b) the hydrophobic surfaces over time.

Whereas the silica nanoparticle concentration and oxygen plasma treatments seemed to have little effect on the initial wettability, these processes had a more significant effect on the surface stability, as only the AR + 2.5% SiO_2 and OP + 5% SiO_2 surfaces stayed

superhydrophilic for 24 days. In addition, the OP + 2.5% SiO_2 surface stayed superhydrophilic for 17 days, while the AR + 5% SiO_2 surface stayed superhydrophilic for less than 5. Even despite this limited stability, all surfaces with silica nanoparticle films significantly out-performed the stability of AR glass, which exhibited degradation in WCA of nearly 25° over 24 days. Even SB glass, which was initially the most hydrophilic surface condition, degrades to a WCA of nearly 20° within 17 days. Note that the SB glass sample data, which was only measured for 17 days, is plotted alongside the data for the samples that were measured for 24 days since it was a hydrophilic surface.

Since none of the surface conditions yielded true superhydrophobic behavior, the concept of superhydrophobic stability is meaningless for these surface conditions. The wetting properties of all AR and OP hydrophobic surfaces quickly degraded, often by at least 5° within 5 days. The SB + 5% SiO_2 + LSF surface was marginally more stable, as it degraded slower than the AR and OP hydrophobic surfaces, while the wettability of the SB + 2.5% SiO_2 + LSF surface was stable at 147° for 12 days before beginning a downward trend at 17 days.

4.2.3 Surface Morphology

Where the silica nanoparticle concentration and oxygen plasma treatments had the most marked effect on the surface properties is the surface morphology. SEM micrographs of the effects of these parameters on surface morphology are shown in Figure 23. In addition, SEM micrographs of the SB surface conditions and a bare AR glass surface are shown in Figure 24.

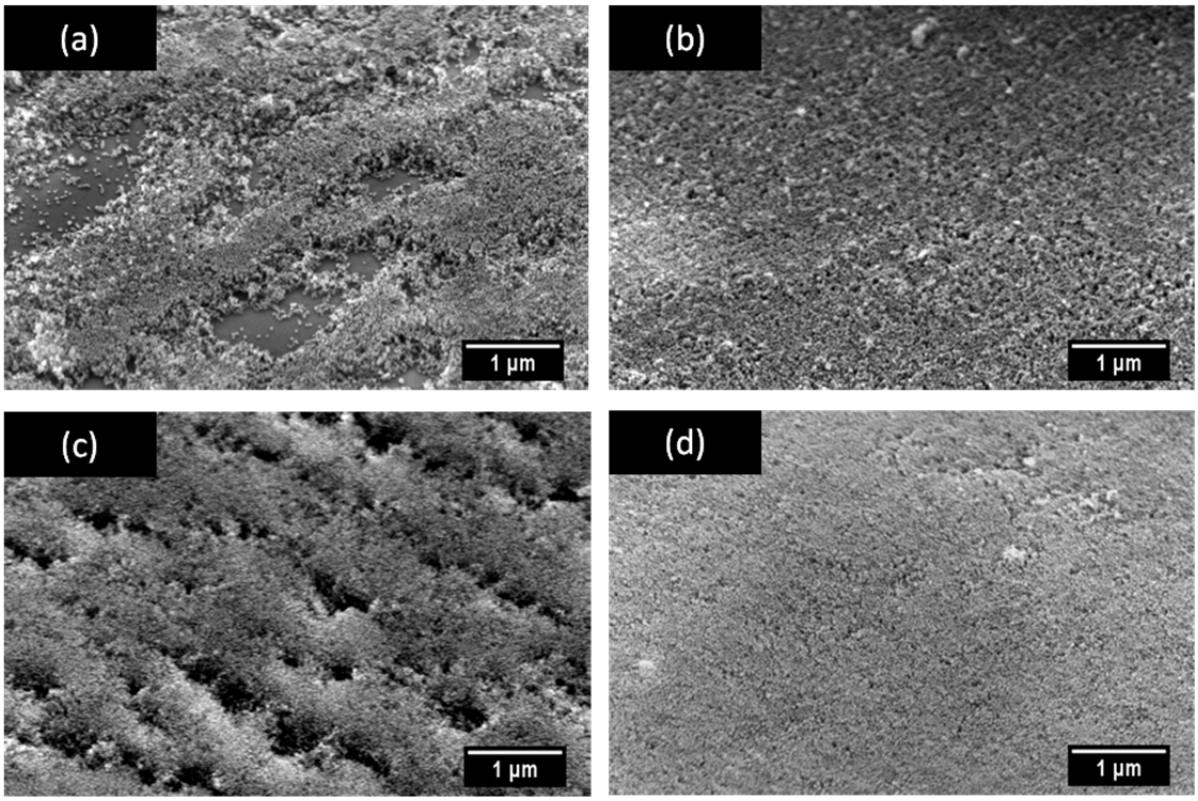

Figure 23: SEM micrographs of the AR + 5% SiO_2 (a), AR + 2.5% SiO_2 (b), OP + 5% SiO_2 (c), and OP + 2.5% SiO_2 (d) glass surfaces, at 20,000× magnification and 45° incidence.

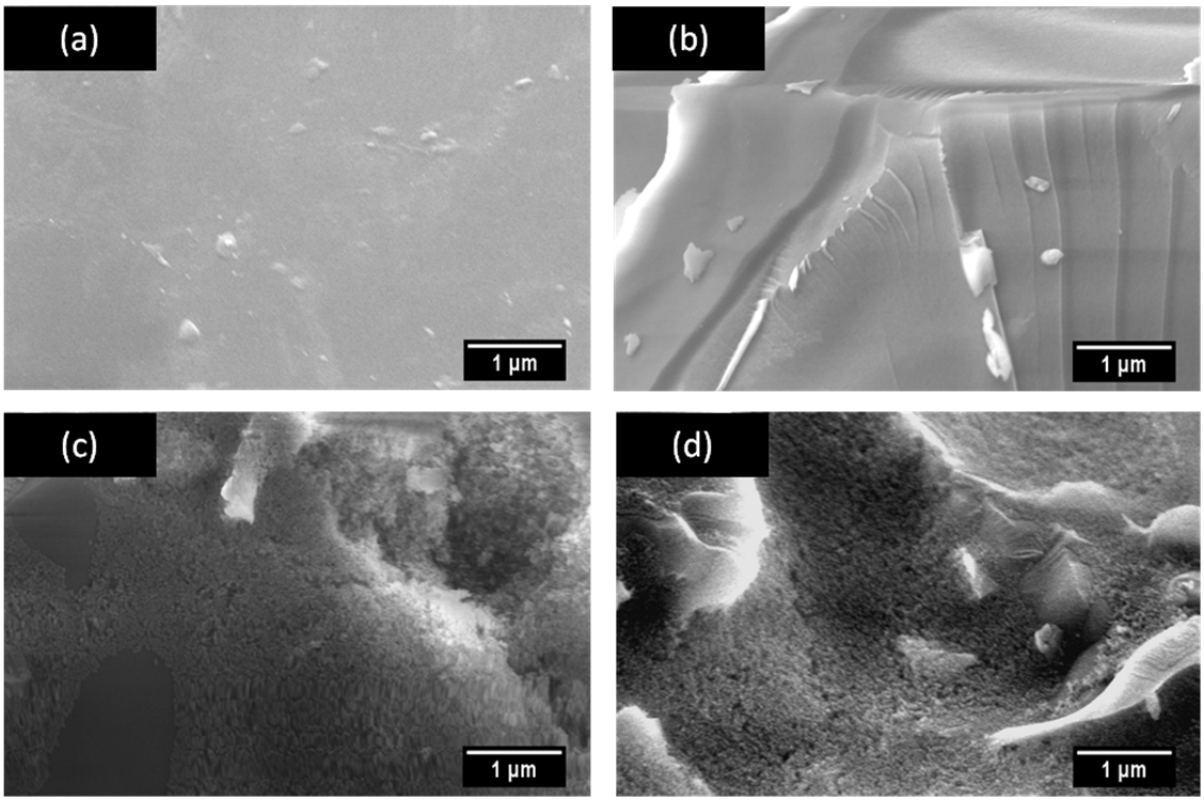

Figure 24: SEM micrographs of the AR (a), SB (b), SB + 5% SiO_2 (c), and SB + 2.5% SiO_2 (d) glass surfaces, at 20,000× magnification and 45° incidence.

As can be seen from Figure 23, silica nanoparticle concentration and oxygen plasma treatments have a demonstrable effect on surface morphology. The nanoparticle coverage of the AR + 5% SiO_2 surface is highly non-uniform, whereas the AR + 2.5% SiO_2 surface displays a much more continuous film. The addition of oxygen plasma treatments results in a much more continuous film on the OP + 5% SiO_2 surface, although large voids in the silica film are still evident, as well as a denser, more-uniform film on the OP + 2.5% SiO_2 surface. The film non-uniformity on the AR + 5% SiO_2 surface is especially significant, as the AR + 5% SiO_2 surface has the worst superhydrophilic stability of all surface conditions containing silica nanoparticles, while the AR + 5% SiO_2 + LSF surface also has the worst hydrophobic stability. The poor wetting properties of these two surfaces are likely a direct result of this surface non-uniformity.

The inability to create superhydrophobic surfaces on glass, even with sandblasting, is also related to the surface morphology. Figure 24 shows that neither the 5% nor 2.5% silica concentrations form continuous nanoparticle films on sandblasted glass. In addition, the SB glass surface is characterized by wide, shallow facets, rather than the peaks and valleys exhibited by sandblasted Ti. These shallow facets and the lack of a hierarchical roughness structure due to incomplete nanoparticle coverage make it very difficult to establish superhydrophobic surfaces through Cassie-Baxter wetting behavior.

4.2.4 Silica Film Thickness Measurements

In addition to surface morphology, the silica nanoparticle concentration and oxygen plasma treatments have a significant effect on the silica nanoparticle film thickness. Film thickness measurements on the AR + 5% SiO_2, AR + 2.5% SiO_2, OP + 5% SiO_2, and OP + 2.5%

SiO_2 glass surfaces are shown in Figure 25. Two samples per surface condition were measured, with 3 measurements per sample, resulting in average values based on 6 measurements.

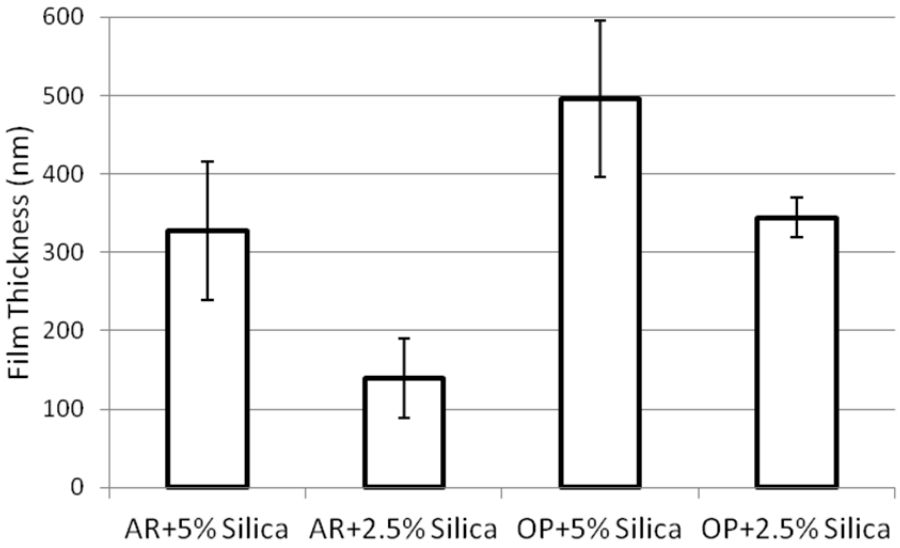

Figure 25: Silica nanoparticle film thicknesses on glass. Error bars denote one standard deviation

The film thickness increases as the silica nanoparticle concentration increases, as the AR + 5% SiO_2 film is roughly 200 nm thicker than the AR + 2.5% SiO_2 film. Notably, oxygen plasma treatments result in a roughly 200 nm increase in film thickness, as can been seen by comparing the OP + 5% SiO_2 and OP + 2.5% SiO_2 surfaces to their non-treated counterparts. This, combined with the effects silica nanoparticle concentration and oxygen plasma treatments have on surface morphology, opens up the possibility to control surface morphology and film thickness by varying the nanoparticle concentration and plasma parameters. The large standard deviations of the AR + 5% SiO_2 and OP + 5% SiO_2 surfaces are related to their non-uniform surface morphologies. Furthermore, the large film thickness is responsible for the

superhydrophilic stability of the OP + 5% SiO_2 surface, which was the best among the glass surface modifications; a large thickness corresponds to increased volume within the nanoporous silica network.

4.2.5 Optical Transmittance Measurements

Optical transmittance measurements on the silica nanoparticle films were conducted to assess their antireflective properties. The use of dielectric materials, such as silica, as antireflective thin films is quite common, in single- and multi-layer arrangements [74]. For a single-layer dielectric film interacting with light at normal incidence in air, the total reflectance will be minimal when [74]

$$n_{film} = \sqrt{n_{air} n_{substrate}} \tag{14}$$

where n_{film}, n_{air}, and $n_{substrate}$ are the indices of refraction of the dielectric film, air, and the substrate, respectively, under the condition that the film thickness is $O(\lambda/4)$, where λ is the wavelength of the light. For $n_{air} \approx 1$ and $n_{substrate} \approx 1.5$ for glass, then $n_{film} \approx 1.225$ is required for optimum optical transmittance. If antireflective behavior is desired across the entire visible spectrum, then this requirement will need to be satisfied on a spectral basis. For dielectric films consisting of nanoparticles, this requirement can be especially difficult to fulfill for all wavelengths in given range since the index of refraction of the nanoparticle film can potentially be a function of thickness, nanoparticle packing density, wavelength, and other contributions.

Optical transmittance spectra of the AR, AR + 5% SiO_2, AR + 2.5% SiO_2, OP + 5% SiO_2, and OP + 2.5% glass surfaces in the visible wavelength regime are shown in Figure 26.

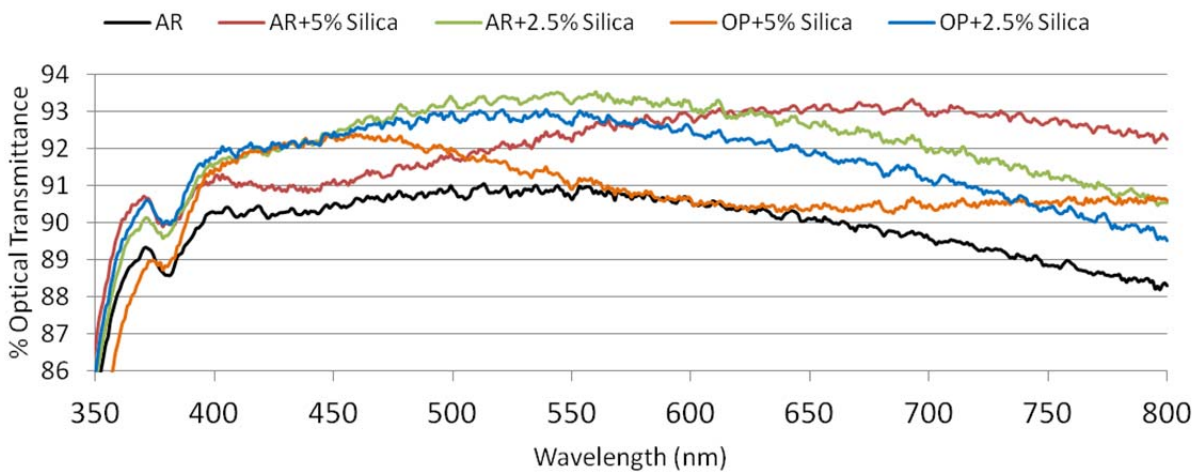

Figure 26: Visible spectrum optical transmittance measurements on the AR, AR + 5% SiO_2, AR + 2.5% SiO_2, OP + 5% SiO_2, and OP + 2.5% glass surfaces.

For the surface conditions measured, the mere presence of a silica nanoparticle film improves optical transmittance in the visible spectrum, regardless of film thickness, morphology, or oxygen plasma treatments. However, no single surface modification provides the best improvement in transmittance across the entire visible spectrum. The AR + 2.5% SiO_2 surface is more antireflective at wavelengths below 600 nm, while the OP + 2.5% SiO_2 surface is more antireflective above this wavelength. The AR + 5% SiO_2 and OP + 5% SiO_2 surfaces display anomalous local minima in the transmittance spectra at roughly 450 nm and 600 nm, respectively. Incidentally, those wavelengths are near to the measured film thicknesses for those surface conditions, so the presence of the local minima could be due to both thin film interference effects related to the wavelength of light being equal to the film thickness, as well as the non-uniform surface morphology exhibited by those surface conditions.

4.3 PET Surface Modifications

4.3.1 Surface Wettability

The average WCAs of the 6 PET surface conditions listed in Table 1 were measured to determine the initial wettabilities of these surfaces. Three samples of each surface condition were measured, with 3 WCAs per sample, resulting in an average based upon 9 WCA measurements. The results are summarized in Figure 27, which shows optical images of representative surface wetting behavior, along with the average WCAs, for each surface condition.

As-received PET has an average WCA of 73°. This can be modified to 42° through oxygen plasma treatments, primarily as a result of the creation of oxygen-based functional groups on the carbon backbone of the PET polymer chains [27]. Neither superhydrophilic nor superhydrophobic behavior is observed for any surface condition. However, nearly superhydrophilic behavior is exhibited by the OP + 5% SiO_2 and OP + 2.5% SiO_2 surfaces, while the OP + 5% SiO_2 + LSF and OP + 2.5% SiO_2 + LSF surfaces are very hydrophobic (WCA ~ 135°). Compared to AR PET, these surface modifications represent significant alterations in the natural surface wettability of PET, despite the lack of true superhydrophilic or superhydrophobic properties. Since no superhydrophilic or superhydrophobic surfaces were achieved for PET substrates, a formal stability analysis was not performed for this material.

4.3.2 Optical Transmittance Measurements

Optical transmittance spectra of the AR, OP + 5% SiO_2, and OP + 2.5% SiO_2 PET surfaces in the visible wavelength regime are shown in Figure 28. Again, the mere presence of a

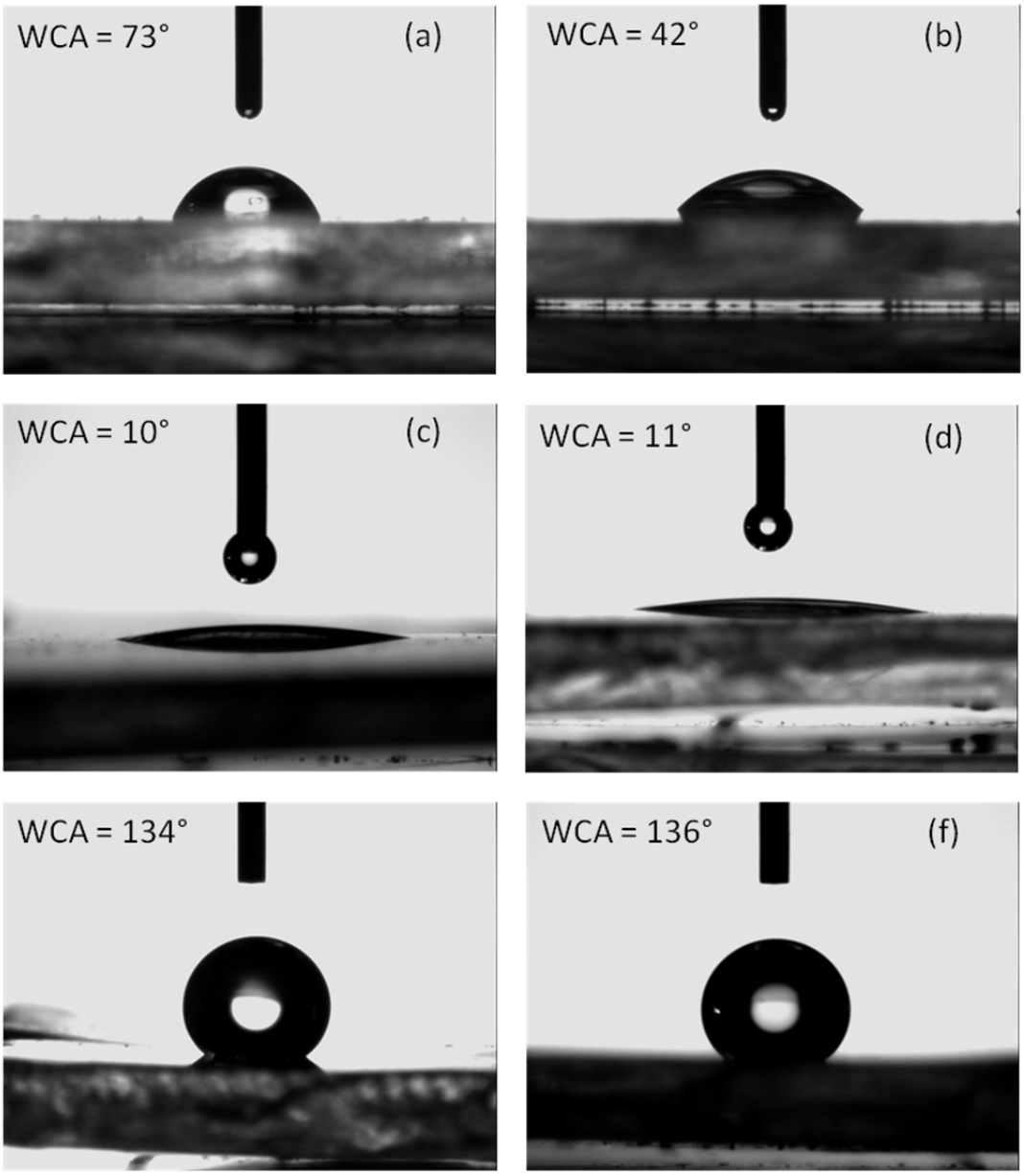

Figure 27: Optical images showing the initial wetting behavior of the AR (a), OP (b), OP + 5% SiO_2 (c), OP + 2.5% SiO_2 (d), OP + 5% SiO_2 + LSF (e), and OP + 2.5% SiO_2 + LSF (f) PET surface conditions, along with average WCA values for each condition.

silica nanoparticle film results in an improvement in optical transmittance in the visible wavelength spectrum. However, in contrast to the transmittance measurements on glass, one of the PET surface modifications provides the best improvement in transmittance across the entire visible spectrum, as the OP + 2.5% SiO_2 surface is more antireflective across the visible spectrum than any of the other surfaces measured. The fact that the silica nanoparticle film is an effective antireflective coating on multiple substrates opens up opportunities to apply these functional surface coatings to other materials of optical interest. In order to utilize such coatings on other substrates, however, it is important to remember that, due to Eq. 14, antireflective properties are not solely due to the film, but are rather a property of the combined film-substrate system.

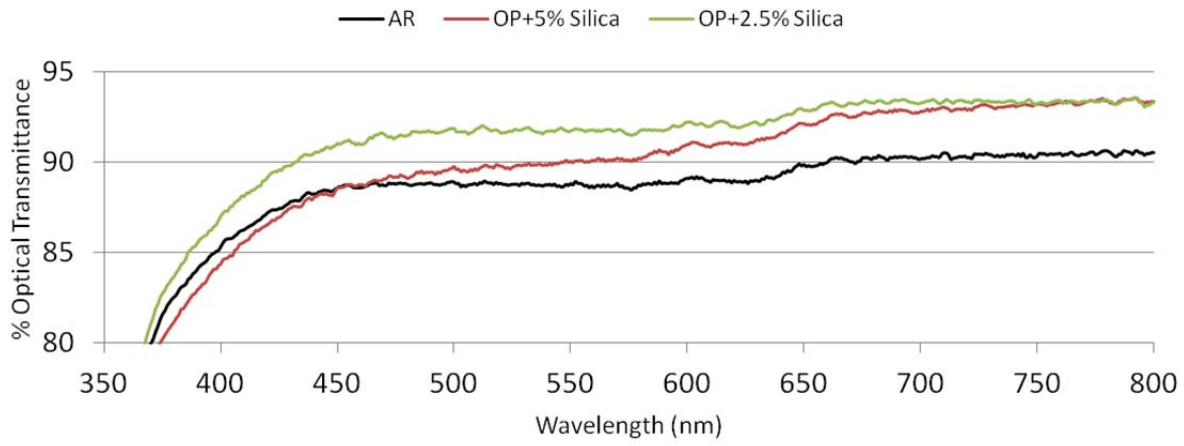

Figure 28: Visible spectrum optical transmittance measurements on the AR, OP + 5% SiO_2, and OP + 2.5% PET surfaces.

V. CONCLUSIONS

5.1 Conclusions

Combinations of sandblasting, oxygen plasma treatments, silica nanoparticle films, and a low SFE fluorocarbon film have been utilized to modify the natural surface wettability of titanium, glass, and PET substrates. These surface modifications have been characterized by their initial wettability, surface wetting stability, surface morphology and roughness, surface elemental compositions, optical transmittance, and other material properties.

The results show that both superhydrophilic and superhydrophobic surfaces can be fabricated on Ti substrates through these methods with long-term stability. The origin of the superhydrophilic behavior is due to a nanoporous network formed by the silica nanoparticle film, while the superhydrophobic behavior is a result of the combination of a micro-nano binary roughness structure and the low SFE film. Moderately stable superhydrophilic surfaces can be produced on glass substrates, with both the initial wetting behavior and stability depending on the surface morphology mediated by the silica nanoparticle concentration and oxygen plasma treatments. Superhydrophobic surfaces on glass were not achieved, primarily due to insufficient surface roughness. Neither superhydrophilic nor superhydrophobic surfaces were exhibited by PET. However, the surface modifications studied were able to elicit very hydrophilic (WCA ~ 10°) or very hydrophobic (WCA ~ 135°) surfaces on PET, representing a significant improvement over the natural wettability of PET (WCA ~ 70°). In addition, the silica nanoparticle films exhibited antireflective behavior, resulting in improved optical transmittance in the visible spectrum compared to bare glass and PET.

This work provides a deeper understanding of the factors that influence the surface wetting behavior and stability of these surface modifications on Ti, glass, and PET, with emphasis on how the fabrication methods employed affect surface morphology and roughness, surface elemental composition, silica film thickness, and other properties. In turn, these properties are correlated to the initial surface wettability, surface wetting stability, and optical transmittance. The results serve as a foundation for further studies into the implementation of these modified surfaces into practical applications, such as biomedical and photovoltaic applications.

5.2 Future Research Directions

5.2.1 Implementation of Ti Surface Modifications for Biomedical Applications

Titanium is frequently used in the field of prosthetic dentistry, owing primarily to its biocompatibility and anti-corrosion properties. Studies have shown that superhydrophilic surfaces can improve cell adhesion [75], which will be beneficial for dental implants. However, a major issue with dental implants is the formation of a bacterial biofilm [76], which can lead to implant failure through inflammation at the implant-tissue interface, known as peri-implantitis [77]. Silver nanoparticles have been widely used as anti-bacterial biocides [78], with the anti-bacterial action mediated by Ag ion release [79]. This presents an opportunity to incorporate Ag nanoparticles into superhydrophilic surfaces to improve cell adhesion and reduce biofilm formation for dental implant applications. In addition, superhydrophobic surfaces on Ti (both with and without Ag nanoparticles) can be investigated for general anti-bacterial applications, due to the low cell adhesion exhibited by superhydrophobic surfaces. For implant applications, the cytotoxicity of the silica nanoparticle film will need to be explicitly investigated.

5.2.2 Implementation of Superhydrophilic Glass for Photovoltaic Applications

A major issue with photovoltaic packages is the contamination of the solar cell surfaces by environmental debris such as dust, with the attendant loss of device efficiency due to this contamination. Superhydrophilic surfaces often exhibit self-cleaning behavior. This, combined with the antireflective properties of the silica nanoparticle film used to induce superhydrophilicity, would be beneficial for implementation in solar cell packaging applications to mitigate the cell efficiency losses due to cell reflectivity and build-up of environmental contaminants. In order to implement the superhydrophilic glass surface detailed in this study for solar cell applications, the self-cleaning properties of this surface modification must first be established and characterized. If such behavior exists, then investigating methods to effectively integrate this superhydrophilic glass surface into actual solar cell packages would be a worthwhile endeavor.

5.2.3 Optimization of Optical Properties of Silica Nanoparticle Films

To truly optimize the antireflective properties of the silica nanoparticle film, the index of refraction of the film must satisfy Eq. 14. In general, the index of refraction of a nanoparticle film will be different from that of a bulk material of the same composition, and potentially depends on the physical properties of the nanoparticle film such as thickness and morphology. It may even have a spectral dependence. In order to design nanoparticle films with maximum optical transmittance, the spectral index of refraction as a function of physical film properties must be determined, either through an experimental framework such ellipsometry or interferometry, or through a first-principles dielectric function calculation. This information,

combined with methods to control film thickness, nanoparticle density, surface morphology/roughness, and other surface properties, would enable the fabrication of nanoparticle films with truly optimum optical properties.

5.2.4 Patterned Superhydrophilic/Superhydrophobic Surfaces

Motivated by the continued advancement in micro/nanotechnology, there is much demand for superhydrophilic and superhydrophobic surfaces that can be accurately patterned, preferably with small spatial resolution and with a sharp interface between the superhydrophilic and superhydrophobic areas [80, 81]. The fabrication methods presented in this study are not amenable to patterning by conventional photolithography, due to an incompatibility between the low SFE fluorocarbon film and the solvents used to remove excess photoresist after patterning. This will result in the change of the superhydrophobic areas to standard hydrophobic behavior, as well as producing an inconsistent interface between the superhydrophilic and hydrophobic areas. If a method of reliably patterning the surfaces reported in this study without compromising the surface wetting properties or interface, such as a physical contact mask or dry photolithography technique, could be developed, then these surfaces could be used to confine, direct, and otherwise manipulate the behavior of liquids on the patterned surface. Such surfaces have potential for applications such as using the surface tension of liquid as a load-bearing mechanism [82, 83], improving microfluidic devices [13, 14, 84], biomimetic surfaces [40, 41], microarrays for biological diagnostics of DNA, proteins, and cells [85], and other novel applications.

REFERENCES

[1] Ozin, G., and Arsenault, A., 2005, "Nanochemistry: A Chemical Approach to Nanomaterials," RSC Publishing.

[2] Hartland, S., 2004, "Surface and Interfacial Tension: Measurement, Theory, and Applications," Marcell Dekker, New York, NY.

[3] Mate, C.M., 2008, "Tribology on the Small Scale," Oxford University Press, .

[4] Suzuki, T., Sugihara, N., Iguchi, E., 2007, "Measurement of Specific Surface Free Energy of Ruby and Quartz Single Crystals using Contact Angle of Liquids," Crystal Research and Technology, **42**(12) pp. 1217-21.

[5] Wenzel, R. N., 1936, "Resistance of Solid Surfaces to Wetting by Water," Industrial and Engineering Chemistry, **28**pp. 988-994.

[6] Cassie, A. B. D., and Baxter, S., 1944, "Wettability of Porous Surfaces," Transactions of the Faraday Society, **40**pp. 546-551.

[7] Nilsson, M. A., Daniello, R. J., and Rothstein, J. P., 2010, "A Novel and Inexpensive Technique for Creating Superhydrophobic Surfaces using Teflon and Sandpaper," Journal of Physics D: Applied Physics, **43**(4) pp. 045301 (5 pp.).

[8] Song, Y., Nair, R. P., Zou, M., 2009, "Superhydrophobic Surfaces Produced by Applying a Self Assembled Monolayer to Silicon micro/nano-Textured Surfaces," Nano Research, **2**(2) pp. 143-50.

[9] Bhushan, B., 2005, "Nanotribology and Nanomechanics: An Introduction," Springer-Verlag Berlin Heidelberg.

[10] Song, Y., Nair, R. P., and Zou, M., 2007, "Hydrophobic surfaces prepared by aluminum-induced crystallization of amorphous silicon," International Conference on Integration and Commercialization of Micro and Nanosystems 2007, January 10 - 13, 2007, Sanya, Hainan, China, **B,** pp. 1537-1540.

[11] Kollias, K., Wang, H., Song, Y., 2008, "Production of a Superhydrophilic Surface by Aluminum-Induced Crystallization of Amorphous Silicon," Nanotechnology, **19**(46) pp. 465304 (6 pp.).

[12] Asthana, Y., and Dong-Pyo Kim, 2006, "A Novel Formulation for the Modification of Transition Metal Oxide Surfaces for Antifogging Optical Application," Materials Science Forum, **510-511**pp. 42-5.

[13] Oliveira, N. M., Neto, A. I., Song, W., 2010, "Two-Dimensional Open Microfluidic Devices by Tuning the Wettability on Patterned Superhydrophobic Polymeric Surface," Applied Physics Express, **3**(8).

[14] Xu, Q. F., Wang, J. N., Smith, I. H., 2008, "Directing the Transportation of a Water Droplet on a Patterned Superhydrophobic Surface," Applied Physics Letters, **93**(23).

[15] Rupp, F., Scheideier, L., Olshanska, N., 2006, "Enhancing Surface Free Energy and Hydrophilicity through Chemical Modification of Microstructured Titanium Implant Surfaces," Journal of Biomedical Materials Research - Part A, **76**(2) pp. 323-334.

[16] Chun, Y., Levi, D. S., Mohanchandra, K. P., 2009, "Superhydrophilic Surface Treatment for Thin Film NiTi Vascular Applications," Materials Science & Engineering: C (Materials for Biological Applications), **29**(8) pp. 2436-41.

[17] Iwasa, F., Hori, N., Ueno, T., 2010, "Enhancement of Osteoblast Adhesion to UV-Photofunctionalized Titanium Via an Electrostatic Mechanism," Biomaterials, **31**(10) pp. 2717-2727.

[18] Gao, S., Zhou, K., Lei, M., 2009, "Comparative Study of the Superhydrophobic-Modification of Silicone Rubber Surfaces by CF4 ICP and CCP," Plasma Processes and Polymers, **6**(8) pp. 530-536.

[19] Cao, L., Jones, A. K., Sikka, V. K., 2009, "Anti-Icing Superhydrophobic Coatings," Langmuir, **25**(21) pp. 12444-12448.

[20] Daoud, W. A., Xin, J. H., and Tao, X., 2004, "Superhydrophobic Silica Nanocomposite Coating by a Low-Temperature Process," Journal of the American Ceramic Society, **87**(9) pp. 1782-4.

[21] Daoud, W. A., Xin, J. H., Zhang, Y. H., 2006, "Pulsed Laser Deposition of Superhydrophobic Thin Teflon Films on Cellulosic Fibers," Thin Solid Films, **515**(2) pp. 835-837.

[22] Gao, Y., Huang, Y., Feng, S., 2010, "Novel Superhydrophobic and Highly Oleophobic PFPE-Modified Silica Nanocomposite," Journal of Materials Science, **45**(2) pp. 460-466.

[23] Douglass, M. R., 1998, "Lifetime estimates and unique failure mechanisms of the Digital Micromirror Device (DMD)," Proceedings of the 1998 36th IEEE International Reliability Physics Symposium, March 31 - April 2, 1998, Reno, NV, USA, pp. 9-16.

[24] Douglass, M. R., 2003, "DMD reliability: A MEMS success story," Reliability, Testing, and Characterization of MEMS/MOEMS II, January 27 - 29, 2003, San Jose, CA, United states, **4980,** pp. 1-11.

[25] Hansman Jr., R. J., and Barsotti, M. F., 1985, "Surface Wetting Effects on a Laminar Flow Airfoil in Simulated Heavy Rain," Journal of Aircraft, **22**(12) pp. 1049-1053.

[26] Thompson, B. E., and Jang, J., 1996, "Surface wettability of wings in rain," Proceedings of the 1996 ASME Fluids Engineering Division Summer Meeting. July 7, 1996 - July 11, San Diego, CA, USA, **237,** pp. 211-216.

[27] Junkar, I., Vesel, A., Cvelbar, U., 2009, "Influence of Oxygen and Nitrogen Plasma Treatment on Polyethylene Terephthalate (PET) Polymers," Vacuum, **84**(1) pp. 83-85.

[28] Li, X., Du, X., and He, J., 2010, "Self-Cleaning Antireflective Coatings Assembled from Peculiar Mesoporous Silica Nanoparticles," Langmuir, **26**(16) pp. 13528-13534.

[29] Beckford, S., and Zou, M., 2011, "Micro/nano engineering on stainless steel substrates to produce superhydrophobic surfaces," Anonymous Elsevier, P.O. Box 211, Amsterdam, 1000 AE, Netherlands, **520,** pp. 1520-1524.

[30] Gao, L., McCarthy, T. J., and Zhang, X., 2009, "Wetting and Superhydrophobicity," Langmuir, **25**(24) pp. 14100-14104.

[31] Guglielmi, M., and Zenezini, S., 1990, "Thickness of Sol-Gel Silica Coatings obtained by Dipping," Journal of Non-Crystalline Solids, **121**(1-3) pp. 303-309.

[32] Attard, G., and Barnes, C., 1998, "Surfaces," Oxford University Press.

[33] Doshi, D. A., Gibaud, A., Liu, N., 2003, "In-Situ X-Ray Scattering Study of Continuous Silica - Surfactant Self-Assembly during Steady-State Dip Coating," Journal of Physical Chemistry B, **107**(31) pp. 7683-7688.
\
[34] Iler, R. K., 1966, "Multilayers of Colloidal Particles," Journal of Colloid and Interface Science, **21**(6) pp. 569-594.

[35] Lee, D., Rubner, M. F., and Cohen, R. E., 2006, "All-Nanoparticle Thin-Film Coatings," Nano Letters, **6**(10) pp. 2305-12.

[36] Cebeci, F. C., Wu, Z., Zhai, L., 2006, "Nanoporosity-Driven Superhydrophilicity: A Means to Create Multifunctional Antifogging Coatings," Langmuir, **22**(6) pp. 2856-2862.

[37] Wang, R., Hashimoto, K., Fujishima, A., 1997, "Light-Induced Amphiphilic Surfaces," Nature, **388**(6641) pp. 431-432.

[38] Fujishima, A., Zhang, X., and Tryk, D. A., 2008, "TiO2 Photocatalysis and Related Surface Phenomena," Surface Science Reports, **63**(12) pp. 515-582.

[39] Permpoon, S., Berthome, G., Baroux, B., 2006, "Natural Superhydrophilicity of Sol-Gel Derived SiO2-TiO 2 Composite Films," Journal of Materials Science, **41**(22) pp. 7650-7662.

[40] Garrod, R. P., Harris, L. G., Schofield, W. C. E., 2007, "Mimicking a Stenocara Beetle's Back for Microcondensation using Plasmachemical Patterned Superhydrophobic-Superhydrophilic Surfaces," Langmuir, **23**(2) pp. 689-693.

[41] Zhai, L., Berg, M. C., Cebeci, F. C., 2006, "Patterned Superhydrophobic Surfaces: Toward a Synthetic Mimic of the Namib Desert Beetle," Nano Letters, **6**(6) pp. 1213-17.

[42] Du, X., Liu, X., Chen, H., 2009, "Facile Fabrication of Raspberry-Like Composite Nanoparticles and their Application as Building Blocks for Constructing Superhydrophilic Coatings," Journal of Physical Chemistry C, **113**(21) pp. 9063-9070.

[43] Liu, X., and He, J., 2007, "Hierarchically Structured Superhydrophilic Coatings Fabricated by Self-Assembling Raspberry-Like Silica Nanospheres," Journal of Colloid and Interface Science, **314**(1) pp. 341-345.

[44] Barthlott, W., and Neinhuis, C., 2001, "Lotus Effect: Nature's Model for Self-Cleaning Surfaces," International Textile Bulletin, **47**(1) pp. 8-8.

[45] Saison, T., Peroz, C., Chauveau, V., 2008, "Replication of Butterfly Wing and Natural Lotus Leaf Structures by Nanoimprint on Silica Sol-Gel Films," Bioinspiration & Biomimetics, **3**(4) pp. 046004 (5 pp.).

[46] Rao, A. V., Latthe, S. S., Dhere, S. L., 2010, "Control on Wetting Properties of Spin-Deposited Silica Films by Surface Silylation Method," Applied Surface Science, **256**(7) pp. 2115-2121.

[47] Han, J. T., Kim, S., and Karim, A., 2007, "UVO-Tunable Superhydrophobic to Superhydrophilic Wetting Transition on Biomimetic Nanostructured Surfaces," Langmuir, **23**(5) pp. 2608-2614.

[48] Cao, L., Hu, H., and Gao, D., 2007, "Design and Fabrication of Micro-Textures for Inducing a Superhydrophobic Behavior on Hydrophilic Materials," Langmuir, **23**(8) pp. 4310-4314.

[49] Song, Y., and Zou, M., 2007, "Superhydrophobic Surfaces by Dynamic Nanomasking and Deep Reactive Ion Etching," Proceedings of the Institution of Mechanical Engineers, Part N (Journal of Nanoengineering and Nanosystems), **221**(2) pp. 41-8.

[50] Zhou, Y., Wang, B., Song, X., 2006, "Control Over the Wettability of Amorphous Carbon Films in a Large Range from Hydrophilicity to Super-Hydrophobicity," Applied Surface Science, **253**(5) pp. 2690-2694.

[51] Guo, Z., Liang, J., Fang, J., 2007, "A Novel Approach to the Robust Ti6Al4V-Based Superhydrophobic Surface with Crater-Like Structure," Advanced Engineering Materials, **9**(4) pp. 316-21.

[52] Mills, A., and Crow, M., 2007, "In Situ, Continuous Monitoring of the Photoinduced Superhydrophilic Effect: Influence of UV-Type and Ambient Atmospheric and Droplet Composition," Journal of Physical Chemistry C, **111**(16) pp. 6009-6016.

[53] Mirshekari, M., Azimirad, R., and Moshfegh, A. Z., 2010, "Superhydrophilic Stability Enhancement of RF Co-Sputtered TixSi1-xO2 Thin Films in Dark," Applied Surface Science, **256**(8) pp. 2500-2506.

[54] Ganjoo, S., Azimirad, R., Akhavan, O., 2009, "Persistent Superhydrophilicity of Sol-Gel Derived Nanoporous Silica Thin Films," Journal of Physics D: Applied Physics, **42**(2).

[55] Xiangmei, L., and Junhui, H., 2009, "Superhydrophilic and Antireflective Properties of Silica Nanoparticle Coatings Fabricated Via Layer-by-Layer Assembly and Postcalcination," Journal of Physical Chemistry C, **113**(1) pp. 148-152.

[56] Du, Y., Luna, L. E., Tan, W. S., 2010, "Hollow Silica Nanoparticles in UV - Visible Antireflection Coatings for Poly(Methyl Methacrylate) Substrates," ACS Nano, **4**(7) pp. 4308-4316.

[57] Dhere, S. L., Latthe, S. S., Kappenstein, C., 2010, "Transparent Water Repellent Silica Films by Sol-Gel Process," Applied Surface Science, **256**(11) pp. 3624-9.

[58] Latthe, S. S., Dhere, S. L., Kappenstein, C., 2010, "Sliding Behavior of Water Drops on Sol-Gel Derived Hydrophobic Silica Films," Applied Surface Science, **256**(10) pp. 3259-3264.

[59] Ferrara, M. C., Pilloni, L., Mazzarelli, S., 2010, "Hydrophilic and Optical Properties of Nanostructured Titania Prepared by Sol-Gel Dip Coating," Journal of Physics D: Applied Physics, **43**(9) pp. 095301 (9 pp.).

[60] Liu, Z., Zhang, X., Murakami, T., 2008, "Sol-Gel SiO2/TiO2 Bilayer Films with Self-Cleaning and Antireflection Properties," Solar Energy Materials and Solar Cells, **92**(11) pp. 1434-8.

[61] Chen, D., Tan, L., Liu, H., 2010, "Fabricating Superhydrophilic Wool Fabrics," Langmuir, **26**(7) pp. 4675-4679.

[62] Aksakal, B., and Hanyaloglu, C., 2008, "Bioceramic Dip-Coating on Ti-6Al-4V and 316L SS Implant Materials," Journal of Materials Science: Materials in Medicine, **19**(5) pp. 2097-2104.

[63] Bienias, J., Surowska, B., Stoch, A., 2009, "The Influence of SiO2 and SiO2-TiO2 Intermediate Coatings on Bond Strength of Titanium and Ti6Al4V Alloy to Dental Porcelain," Dental Materials, **25**(9) pp. 1128-1135.

[64] Nakatani, T., Okamoto, K., Omura, I., 2007, "Imparting Superhydrophilicity to Diamond-Like Carbon by Plasma Surface Treatment Technique," New Diamond and Frontier Carbon Technology, **17**(6) pp. 289-300.

[65] Madou, M.J., 2002, "Fundamentals of Microfabrication: The Science of Miniaturization," CRC Press, Boca Raton, FL.

[66] Goldstein, J., Newbury, D., Joy, D., 2003, "Scanning Electron Microscopy and X-Ray Microanalysis," Springer Science + Business Media, New York, NY.

[67] Brundle, C.R., Evans, C.A., and Wilson, S., 1992, "Encyclopedia of Materials Characterization," Butterworth-Heineman.

[68] Clegg, W., 1997, "Crystal Structure Determination," Oxford University Press.

[69] Cullity, B.D., 1978, "Elements of X-Ray Diffraction," Addison-Wesley Publishing Company.

[70] Kroemer, H., 1994, "Quantum Mechanics: For Engineering, Materials Science, and Applied Physics," Prentice-Hall, Upper Saddle River, NJ.

[71] Fox, M., 2001, "Optical Properties of Solids," Oxford University Press.

[72] Iler, R. K., 1979, "Chemistry of Silica - Solubility, Polymerization, Colloid and Surface Properties and Biochemistry," John Wiley & Sons.

[73] Takaba, H., Katagiri, M., Kubo, M., 1995, "Theoretical Studies on the Affinity of CO2 and N2 Molecules to Solid Surfaces," Energy Conversion and Management, **36**(6-9) pp. 439-442.

[74] Hecht, E., 2002, "Optics," Addison Wesley Publishing Company.

[75] Ishizaki, T., Saito, N., and Takai, O., 2010, "Correlation of Cell Adhesive Behaviors on Superhydrophobic, Superhydrophilic, and Micropatterned superhydrophobic/superhydrophilic Surfaces to their Surface Chemistry," Langmuir, **26**(11) pp. 8147-8154.

[76] Busscher, H. J., Rinastiti, M., Siswomihardjo, W., 2010, "Biofilm Formation on Dental Restorative and Implant Materials," Journal of Dental Research, **89**(7) pp. 657-665.

[77] Heitz-Mayfield, L., and Lang, N. P., 2010, "Comparative Biology of Chronic and Aggressive Periodontitis Vs. Peri-Implantitis," Periodontology 2000, **53**(1) pp. 167-181.

[78] Flores, C. Y., Diaz, C., Rubert, A., 2010, "Spontaneous Adsorption of Silver Nanoparticles on Ti/TiO2 Surfaces. Antibacterial Effect on Pseudomonas Aeruginosa," Journal of Colloid & Interface Science, **350**(2) pp. 402-408.

[79] Damm, C., 2005, "Silver Ion Release from Polymethyl Methacrylate Silver Nanocomposites," Polymers and Polymer Composites, **13**(7) pp. 649-656.

[80] Bhushan, B., Nosonovsky, M., and Yong, C. J., 2007, "Towards Optimization of Patterned Superhydrophobic Surfaces," Journal of the Royal Society Interface, **4**(15) pp. 643-8.

[81] Kietzig, A., Hatzikiriakos, S. G., and Englezos, P., 2009, "Patterned Superhydrophobic Metallic Surfaces," Langmuir, **25**(8) pp. 4821-4827.

[82] Chappuis, J., 1982, "Lubrication by a New Principle: The Use of Non-wetting Liquids," Wear, **77**(3) pp. 303-313.

[83] Choo, J. H., Glovnea, R. P., Forrest, A. K., 2007, "A Low Friction Bearing Based on Liquid Slip at the Wall," Journal of Tribology, **129**(3) pp. 611-620.

[84] Takei, G., Nonogi, M., Hibara, A., 2007, "Tuning Microchannel Wettability and Fabrication of Multiple-Step Laplace Valves," Lab on a Chip, **7**(5) pp. 596-602.

[85] Zhang, H., Lee, Y. Y., Leck, K. J., 2007, "Recyclable Hydrophilic-Hydrophobic Micropatterns on Glass for Microarray Applications," Langmuir, **23**(9) pp. 4728-4731.